Research Paper

GEOSPHERE

GEOSPHERE

https://doi.org/10.1130/GES02574.1

7 figures (2 figures are interactive); 3 tables; 1 set of supplemental files

CORRESPONDENCE: lee1@mines.edu

CITATION: Lee, J., Stockli, D.F., and Blythe A.E., 2023, Cenozoic slip along the southern Sierra Nevada normal fault, California (USA): A long-lived stable western boundary of the Basin and Range: Geosphere, https://doi.org/10.1130/GES02574.1.

Science Editor: Christopher J. Spencer

Received 20 July 2022
Revision received 17 January 2023
Accepted 13 February 2023

Published online 28 April 2023

Cenozoic slip along the southern Sierra Nevada normal fault, California (USA): A long-lived stable western boundary of the Basin and Range

Jeffrey Lee[1,2], Daniel F. Stockli[3], and Ann E. Blythe[4]

[1]Department of Geological Sciences, Central Washington University, Ellensburg, Washington 98926, USA
[2]Department of Geophysics, Colorado School of Mines, Golden, Colorado 80401, USA
[3]Department of Geological Sciences, University of Texas, Austin, Texas 78712, USA
[4]Department of Geology, Occidental College, Los Angeles, California 90041, USA

ABSTRACT

The uplift history of the Sierra Nevada, California, is a topic of long-standing disagreement with much of it centered on the timing and nature of slip along the range-bounding normal fault along the east flank of the southern Sierra Nevada. The history of normal fault slip is important for characterizing the uplift history of the Sierra Nevada, as well as for characterizing the geologic and geodynamic factors that drove, and continue to drive, normal faulting. To address these issues, we completed new structural studies and extensive apatite (U-Th)/He (AHe) thermochronometry on samples collected from three vertical transects in the footwall to the east-dipping southern Sierra Nevada normal fault (SNNF). Our structural studies on bedrock fault planes show that the SNNF is a steeply (~70°) east-dipping normal fault. The new AHe data reveal two elevation-invariant AHe age arrays, indicative of two distinct periods of cooling and exhumation, which we interpret as initiation of normal faulting along the SNNF at ca. 28–27 Ma with a second phase of normal faulting at ca. 17–13 Ma. We argue that beginning in the late Oligocene, the SNNF marked the now long-standing stable western limit, or break-away zone, of the Basin and Range. Slip along SNNF, and the associated unloading of the footwall, likely resulted in two periods of uplift of Sierra Nevada during the late Cenozoic. Trench retreat, driven by westward motion of the North American plate, along the Farallon–North American subduction zone boundary, as well as the gravitationally unstable northern and southern Basin and Range pushing on the cold Sierra Nevada, likely drove the late Oligocene-aged normal slip along the SNNF and the similar-aged but generally local and minor extension within the Basin and Range. We posit that the thick proto–Basin and Range lithosphere was primed for late Oligocene extension by replacement of the steepening Farallon slab with hot and buoyant asthenosphere. While steepening of the Farallon slab had not yet reached the southern Sierra Nevada by late Oligocene time, we speculate that late Oligocene slip along the SNNF reactivated a late Cretaceous dextral shear zone as the Sierra Nevada block was pulled and pushed westward in response to trench retreat and gravitational potential energy. The dominant middle Miocene normal fault-slip history along the SNNF is contemporaneous with high-magnitude slip recorded along range-bounding normal faults across the Basin and Range, including the east-adjacent Inyo and White mountains, indicating that this period of extension was a major regional tectonic event. We infer that a combination of slab-driven trench retreat along the Juan de Fuca–North America subduction zone boundary and clockwise rotation of the southern ancestral Cascade Range superimposed on continental lithosphere pre-conditioned for extension drove this episode of middle Miocene normal slip along the SNNF and extension to the east across the Basin and Range. Transtensional plate motion along the Pacific–North America plate boundary, and likely a growing slab window, continued to drive extension along the SNNF and the western Basin and Range, but not until ca. 11 Ma when the Mendocino triple junction reached the latitude of our northernmost (U-Th)/He transect.

INTRODUCTION

The topographic development of the Sierra Nevada, California, (Fig. 1) has been the topic of research for more than 100 years (e.g., LeConte, 1886; Lindgren, 1911; Christensen, 1966; Huber, 1981; Poage and Chamberlain, 2002; Wakabayashi, 2013; and many others), yet there remains disagreement as to whether the Sierra Nevada experienced (1) uplift in the late Mesozoic followed by no change or a decrease in elevation throughout the Cenozoic or (2) uplift in the late Mesozoic followed by first a decrease in elevation during the middle Cenozoic and second by a second pulse of uplift in the late Cenozoic. A variety of data sets, including seismic (Wernicke et al., 1996), thermochronometric (e.g., House et al., 1998, 2001), isotopic paleoaltimetry (e.g., Poage and Chamberlain, 2002; Mulch et al., 2006; Cassel et al., 2009), and cutting and filling of paleovalleys (e.g., Cassel and Graham, 2011), underpin the hypothesis that the Sierra Nevada rose in the late Mesozoic and remained high standing since then or lost elevation during most of the Cenozoic. In contrast, other data sets, including a combination of geology and geomorphology (e.g., Christensen, 1966), westward tilting (e.g., Huber, 1981; Hildreth et al., 2022), flexural

Figure 1 is interactive. Maps, labels, and data sets for this figure are organized in a series of layers that may be viewed separately or in combination using the capabilities of the Acrobat (PDF) layering function (click "Layers" icon along vertical bar on left side of window for display of available layers, or turn layers on or off by clicking the box that encompasses the layer label located within the gray box in the lower right corner of the map). To interact with Figure 1 if reading the full-text version of this paper, please visit https://doi.org/10.1130/GEOS.S.22662076.

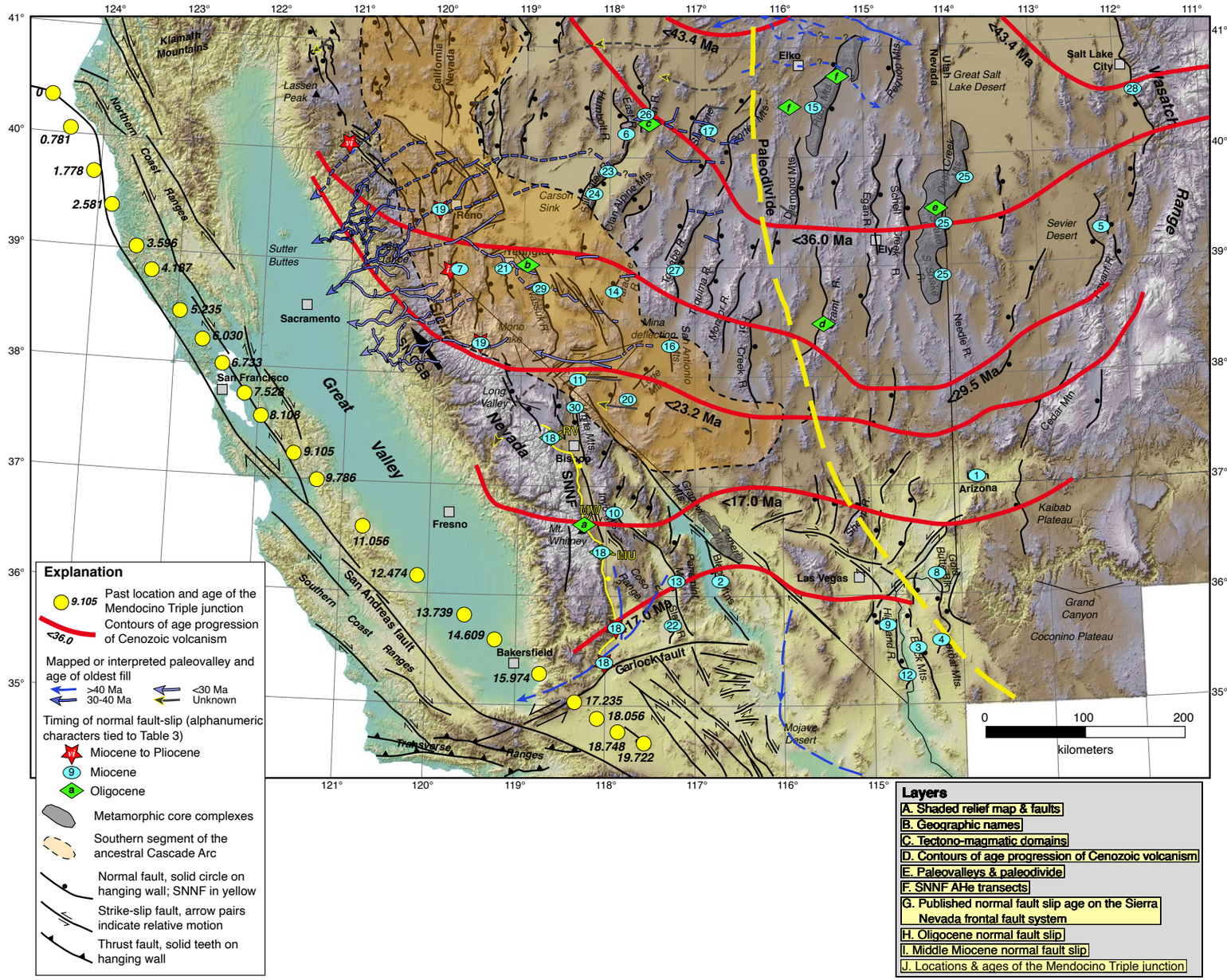

Figure 1 (interactive). Layer A. Digital shaded relief map of California, Nevada, northwestern Arizona, and western Utah, showing major normal, strike-slip, and thrust faults. Heavy black arrow shows the present-day azimuth of motion of the Sierra Nevada block with respect to the central Great Basin (SN-CBG) (Bennett et al., 2003). SNNF—southern Sierra Nevada normal fault. Layer B. Geographic names. Layer C. Outline of the late Eocene to early Pleistocene southern ancestral Cascade magmatic arc (from John et al., 2012; Du Bray et al., 2014), and locations of metamorphic core complexes. Layer D. Contours of age progression of Cenozoic volcanism associated with initiation of Farallon slab rollback (from Konstantinou et al., 2012). Layer E. Mapped or interpreted paleovalleys and oldest volcanic and/or sedimentary fill (from MacGinitie, 1941; Yeend, 1974; Garside et al., 2005; Henry, 2008; Henry et al., 2012, and references therein; Henry and John, 2013; Lee et al., 2020; Lund Snee and Miller, 2022) and inferred Cenozoic paleovalley divide (from Henry, 2008). Layer F. Locations of our apatite (U-Th)/He (AHe) sample transects (Round Valley—RV; Mount Williamson—MW; and Muah Mountain—MU) (bold yellow font) along the SNNF. Layer G. Locations of published Miocene to Pliocene normal fault slip along the Sierra Nevada frontal fault system (red stars). Layer H. Locations of Oligocene initiation of normal fault slip along the SNNF and published Oligocene normal fault slip across the Basin and Range (green diamonds). Layer I. Locations of Miocene normal fault slip along the SNNF and published Miocene to Pliocene normal fault slip across the Basin and Range (light-blue ellipses). Layer J. Past locations and age of the Mendocino Triple junction with respect to North America (noise-reduced locations from DeMets and Merkouriev, 2016). See text Table 3 for timing of normal fault slip for each location in layers H and I. Maps, labels, and data sets for this figure are organized in a series of layers that may be viewed separately or in combination using the capabilities of the Acrobat (PDF) layering function (click "Layers" icon along vertical bar on left side of window for display of available layers, or turn layers on or off by clicking the box that encompasses the layer label located within the gray box in the lower right corner of the map). To interact with Figure 1 if reading the full-text version of this paper, please visit https://doi.org/10.1130/GEOS.S.22662076.

isostasy (e.g., Chase and Wallace, 1986), river incision (e.g., Stock et al., 2004), thermochronometry (e.g., Clark et al., 2005; McPhillips and Brandon, 2012), thermomechanical modeling and geologic data applied to test those model results (Saleeby et al., 2012, 2013), and geodesy (Hammond et al., 2016), support the scenario that the Sierra Nevada underwent an episode of late Cenozoic uplift. Some proponents for a period of late Cenozoic uplift of the Sierra Nevada invoked normal slip along the east-dipping Sierra Nevada frontal fault system to drive at least some of the uplift (e.g., Chase and Wallace, 1986; Thompson and Parsons, 2009; McPhillips and Brandon, 2012; Martel et al., 2014) (Fig. 1A).

Although several publications (e.g., Chase and Wallace, 1986; Thompson and Parsons, 2009; McPhillips and Brandon, 2012; Martel et al., 2014) argued that a period of late Cenozoic uplift of the Sierra Nevada was, at least in part, linked to normal slip along the Sierra Nevada frontal fault system (Fig. 1A), the timing of normal faulting along the southern Sierra Nevada normal fault (SNNF) has not yet been conclusively documented. In light of the uncertainty of the exact timing of late Cenozoic normal slip along the SNNF, several geodynamic processes have been postulated as drivers for normal faulting, including: (1) development of a slab window (e.g., Best and Hamblin, 1978; Dickinson and Snyder, 1979; Atwater and Stock, 1998), (2) oblique transform slip along the Pacific–North American plate boundary (e.g., Atwater, 1970; Best and Christiansen, 1991; Dickinson, 1997, 2002; Atwater and Stock, 1998; Colgan and Henry, 2009), and (3) replacement of foundering dense lithosphere mantle with upwelling asthenosphere beneath the southern Sierra Nevada (e.g., Ducea and Saleeby, 1996; Liu and Shen, 1998; Manley et al., 2000; Farmer et al., 2002; Saleeby et al., 2003; Jones et al., 2004; Zandt et al., 2004).

To quantify the timing of Cenozoic normal slip along the SNNF, assess the link between normal fault slip and uplift, and test the geodynamic processes that are postulated to drive that slip, herein we describe new structural data and present detailed apatite (U-Th)/He (AHe) low-temperature thermochronometric results from the immediate footwall of the SNNF, which forms the steep eastern flank of the Sierra Nevada from about the latitude of Round Valley southward to the Garlock fault (Figs. 1 and 2). Our integrated structure and AHe data constrain the onset of normal fault slip along the steeply east-dipping SNNF to the late Oligocene and document a second, younger, and dominant episode of slip during the middle Miocene. These results have important implications for the timing of surface uplift of the Sierra Nevada and for the geodynamic processes that drove, and continue to drive, extension across the Basin and Range.

TECTONIC AND GEOLOGIC SETTING

The ~600-km-long, ~80–130-km-wide, and >4-km-high Sierra Nevada is characterized by an asymmetric topographic expression with a short, steep eastern flank and a long, shallow western flank. Bedrock exposures in the Sierra Nevada are dominated by Mesozoic granitic plutons (e.g., Bateman and Wahrhaftig, 1966; Saleeby and Sharp, 1980; Stern et al., 1981; Chen and Moore, 1982; Saleeby et al., 2008) that intruded Paleozoic and Mesozoic metasedimentary and metavolcanic rocks (e.g., Bateman and Wahrhaftig, 1966; Saleeby, 1981; Schweickert, 1981; Sharp, 1988). Eocene stream gravels, sourced locally and from Nevada, and Oligocene ignimbrites, sourced from Nevada, were deposited in major east-west–trending river channels that crossed the central and northern Sierra Nevada and debouched into the Great Valley (e.g., Henry and Faulds, 2010; Cassel et al., 2012a; Henry et al., 2012) (Fig. 1C). The absence of Eocene river channels crossing the southern Sierra Nevada may be the consequence of a topographic boundary due to Eocene slip along the normal fault bordering the west flank of the Inyo Mountains and/or normal slip along the proto–Owens Valley fault (Sousa, 2019) (Fig. 1).

Geodetically, the combined Sierra Nevada–Great Valley block defines a single, rigid microplate (e.g., Argus and Gordon, 1991; Dixon et al., 2000) that is located between the transpressional belt in the Coast Ranges (e.g., Page et al., 1998) to the west and the Sierra Nevada frontal fault system along the east flank of the Sierra Nevada to the east (e.g., Bateman, 1965; Bateman and Wahrhaftig, 1966; Wakabayashi and Sawyer, 2001) (Fig. 1). The SNNF defines the western boundary of the Basin and Range Province and Walker Lane (Figs. 1 and 2). In general, this normal fault juxtaposes extensive Quaternary alluvial fan, glacial, and rockslide deposits in the hanging wall upon bedrock in the footwall along the eastern range front (e.g., Bateman, 1965; Berry, 1997; Le et al., 2007) (Fig. 3A); locally, the SNNF cuts Cenozoic volcanic rocks (e.g., Wakabayashi and Sawyer, 2001). Field-based studies show that the SNNF is still active (e.g., Berry, 1997; Le et al., 2007).

FAULT GEOMETRY

The SNNF comprises several, generally left-stepping NNW-striking, east-dipping normal fault segments (e.g., Unruh et al., 2003; Le et al., 2007) (Figs. 1A and 2). To document the average strike and dip of the SNNF, we combined our structural measurements at the range front on well-exposed joints within the first few meters of the footwall and on scarce bedrock fault planes and fault striations exposed along the bedrock footwall–Quaternary deposit hanging-wall contact with published bedrock fault plane measurements (see plate 2 in Bateman, 1965; Stone et al., 2000) at two study areas—Round Valley (RV) and Mount Williamson (MW) (Fig. 3). Bedrock fault planes and fault scarps are not exposed at Muah Mountain (MU) study area. Fault plane and joint measurements from RV yield a spread of strikes from NE to NW, whereas fault plane and joint measurements from MW yield NE-ENE strikes, consistent with the map traces at both localities, respectively. Average fault plane and joint orientations from the combined data sets from RV and MW yield nearly identical strike and dip values of ~357° and 69°NE, respectively, indicating that the SNNF is defined by a steep east dip, and the better exposed joint planes at the range front can be used as a proxy for the strike and dip of the fault plane (Fig. 3B). Our measurements of bedrock fault planes indicate that the SNNF dips steeply east, which is in contrast to the suggestion that in Round Valley

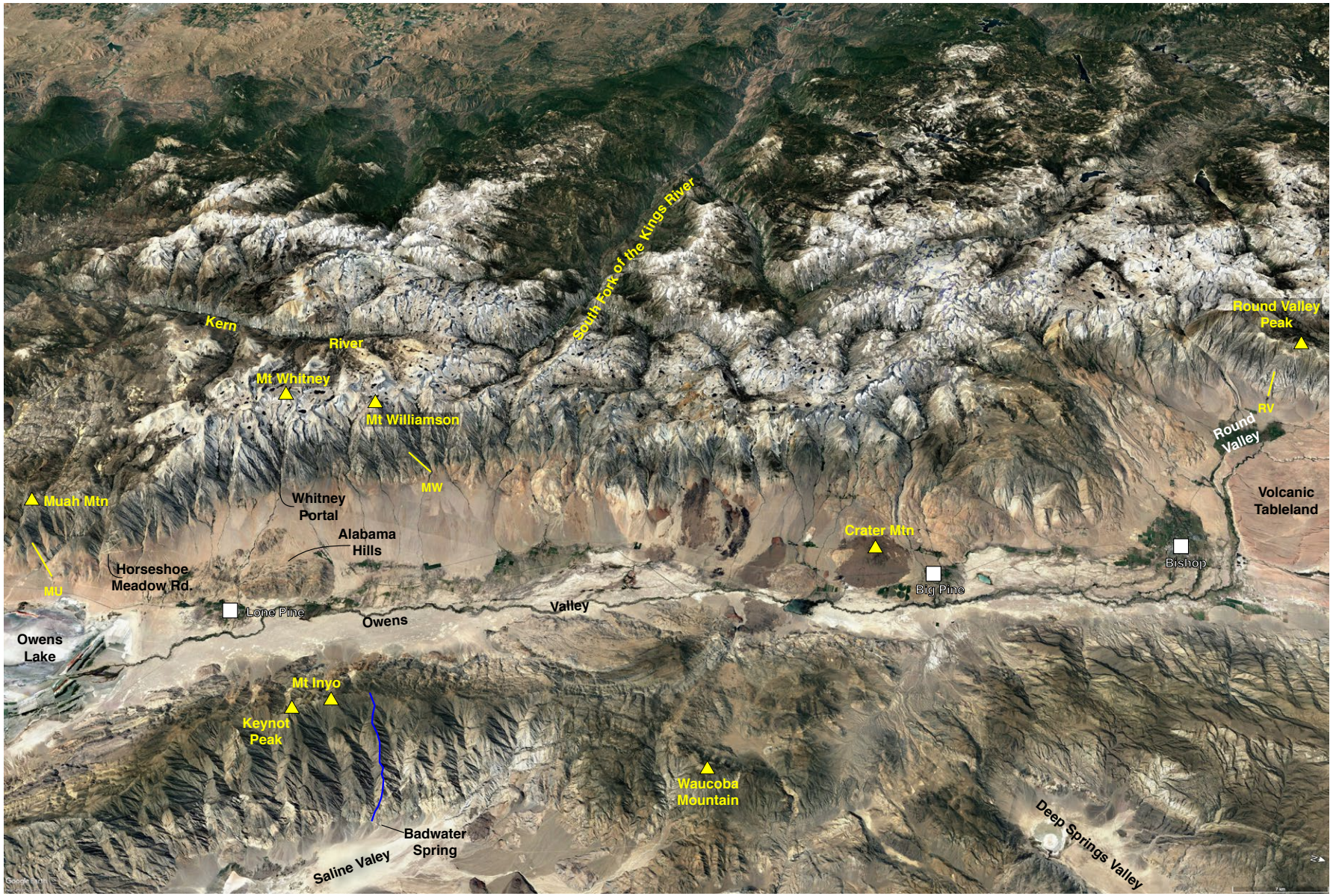

Figure 2. Oblique Google Earth view to the west-southwest of the southern Sierra Nevada from Round Valley Peak in the north to Muah Mountain in the south. Yellow lines show the locations of our three apatite (U-Th)/He (AHe) transects at Round Valley (RV), Mount Williamson (MW), and Muah Mountain (MU). The east-dipping southern Sierra Nevada normal fault (SNNF) is located at the base of the eastern flank of the southern Sierra Nevada. Blue line shows the location of the AHe transect along the eastern flank of the Inyo Mountains (Lee et al., 2009). The east-dipping Eastern Inyo fault zone is located at the base of the eastern flank of the Inyo Mountains.

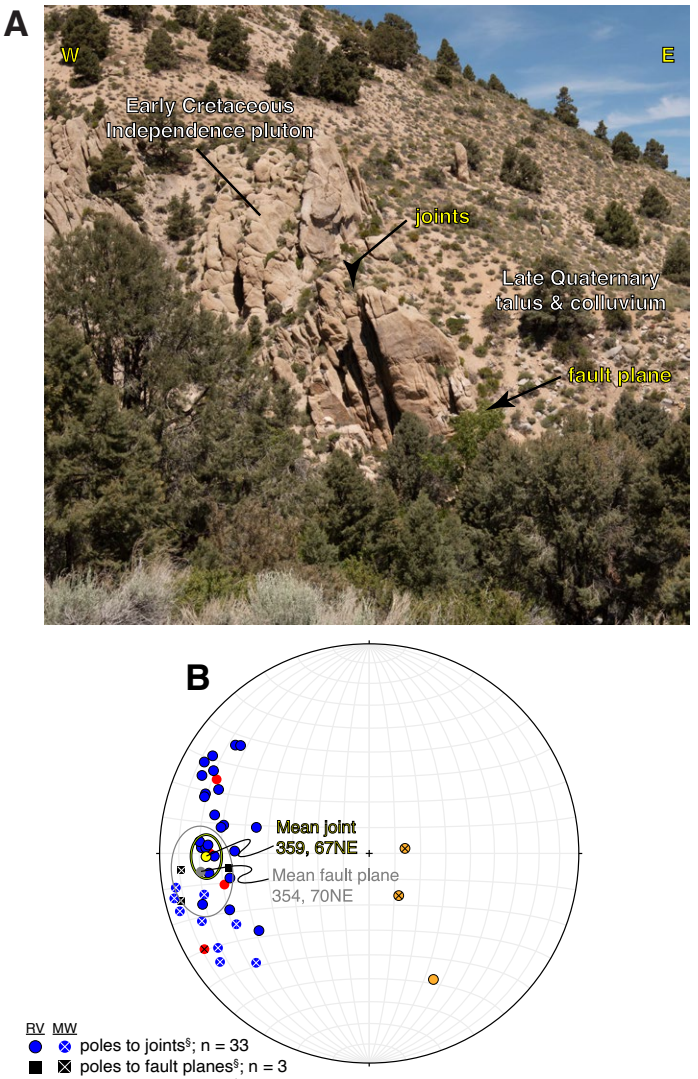

Figure 3. (A) Field photograph of normal fault plane and joints in bedrock at the bedrock footwall–Quaternary deposit hanging-wall fault contact along the southern Sierra Nevada normal fault (SNNF) at the base of the Mount Williamson (MW) transect. Photo view is north across Bairds Creek approximately along strike of the fault plane and joints. (B) Equal area, lower-hemisphere stereonet plot of poles to joints and normal fault planes, and trend and plunge of fault striations from bedrock joints and fault planes exposed along the Round Valley and MW segments of the SNNF.

the fault dips generally shallowly to moderately east based on three-point problems on fault scarps (Phillips and Majkowski, 2011).

APATITE (U-Th)/He AGE RESULTS

To quantify the low-temperature cooling history, and thereby the exhumation and fault-slip history along the SNNF, we completed 352 AHe analyses on 44 apatite samples collected from granitoid rocks exposed in the immediate footwall of the SNNF along three ~802–1043-m-long vertical transects (Round Valley, RV; Mount Williamson, MW; Muah Mountain, MU) distributed ~130 km along strike (Figs. 1, 2, 4, and 5). The elevation–AHe age trends for each transect are shown in Figure 6, and sample ages are tabulated in Table 1; AHe analytical techniques and raw and reduced (U-Th[Sm]/He data results are provided in File S1[1].

AHe thermochronology is a well-established approach to dating the low-temperature cooling histories, with a calculated partial retention zone (PRZ) of ~40–80 °C (e.g., Wolf et al., 1996, 1998; House et al., 1998; Farley, 2000; Stockli et al., 2000). Helium dating of apatite is based on the decay of ^{235}U, ^{238}U, and ^{232}Th by alpha (^{4}He) emission. ^{4}He is completely expelled from apatite at temperatures above ~80 °C, retained below ~40 °C, and partially retained between ~80 and ~40 °C (Wolf et al., 1996, 1998; House et al., 1998; Stockli et al., 2000; Flowers et al., 2009). This thermochronologic technique has been successfully applied in documenting the exhumation histories of the immediate footwall of a normal fault (e.g., Stockli et al., 2002; Colgan et al., 2008; Lee et al., 2009). If normal fault slip has been rapid and of sufficient magnitude to exhume footwall rocks from below the AHe PRZ, AHe ages from samples collected along a vertical transect in the footwall will directly date the timing of footwall exhumation and faulting (e.g., Stockli et al., 2000).

At RV, 15 samples collected from Triassic quartz monzonite and Cretaceous(?) alaskite (see plate 2 in Bateman, 1965) over a vertical distance of ~802 m record AHe ages that range from ca. 12.2 Ma to ca. 28.6 Ma (Figs. 4A, 5A, and 6A). Ages from 13 of these samples spread out over the entire vertical transect overlap, within error, which return a calculated elevation invariant mean age of 17.4 ± 4.6 Ma (2σ error) (Fig. 6A). Three samples from about the middle of the transect yield ages that overlap, within error, and define an elevation invariant mean age of 28.1 ± 2.4 Ma. These ages are older than RV samples above and below, but the same, within error, to several samples in the MW and MU transects (see below). This geometric age relation suggests that these three RV samples are in the hanging wall of a normal fault sliver within the footwall of the SNNF that has duplicated, in part, the middle Oligocene cooling trend. Although an intraplutonic normal fault strand to the west of these samples has not been mapped (Fig. 4; Bateman, 1965), similar

[1]Supplemental Material. File S1: Provides a description of (U-Th)/He analytical techniques and (U-Th)/He analytical results. Table S1: AHe analytical techniques and raw and reduced (U-Th[Sm]/He data results. Please visit https://doi.org/10.1130/GEOS.S.22152095 to access the supplemental material, and contact editing@geosociety.org with any questions.

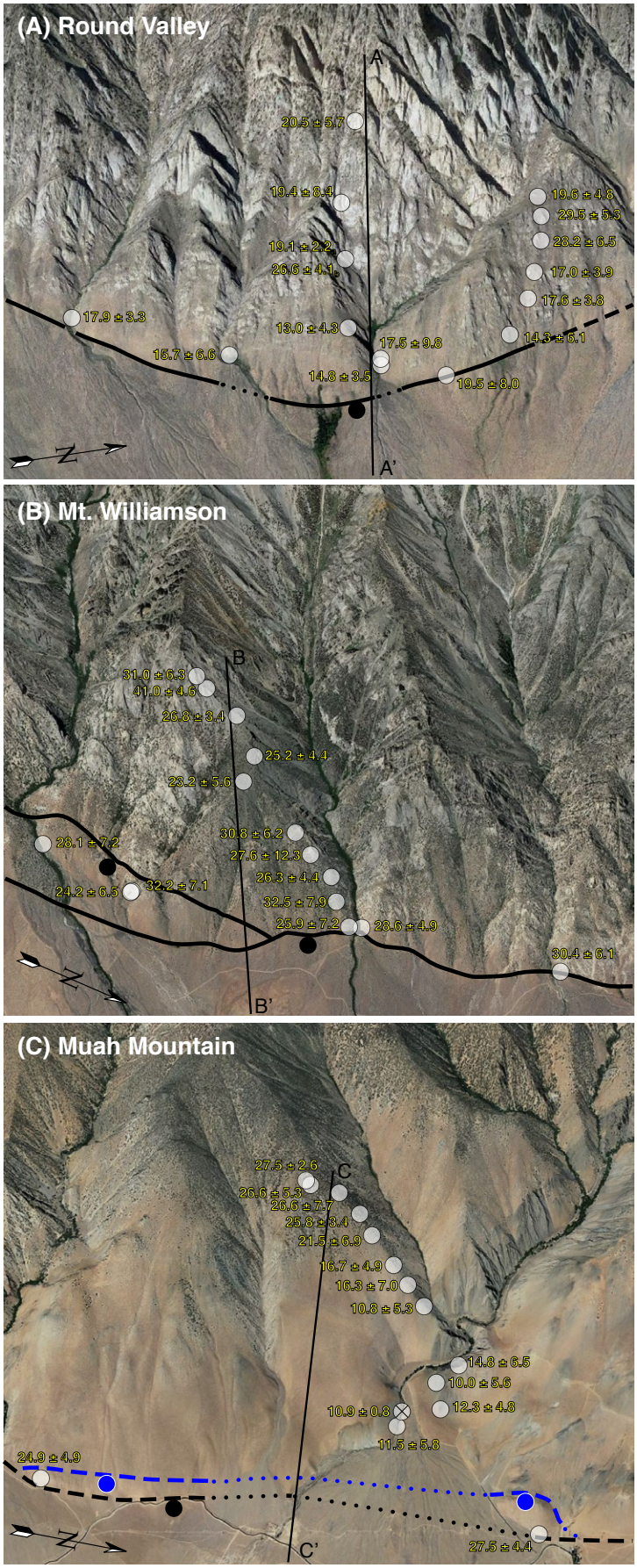

Figure 4. Location of apatite (U-Th)/He (AHe) samples and associated (AHe) ages shown on oblique, 2× vertically exaggerated Google Earth images; view is approximately to the west. (A) Round Valley (RV). For scale, 2.90 km is the horizontal distance between AHe samples with ages of 19.5 ± 8.0 Ma and 17.9 ± 3.3 Ma, and 802 m is the elevation difference between AHe samples with ages 19.5 ± 8.0 Ma and 20.5 ± 5.7 Ma. (B) Mount Williamson (MW). For scale, 5.31 km is the horizontal distance between AHe samples with ages of 30.4 ± 6.1 Ma and 28.1 ± 7.2 Ma, and 984 m is the elevation difference between AHe samples with ages of 28.6 ± 4.9 Ma and 31.0 ± 6.3 Ma. (C) Muah Mountain (MU). For scale, 5.10 km is the horizontal distance between AHe samples with ages of 27.5 ± 4.4 Ma and 24.9 ± 4.9 Ma, and 926 m is the elevation difference between AHe samples with ages of 11.5 ± 5.8 Ma and 27.5 ± 2.6 Ma; "x" on top of semi-transparent circle is an AHe sample from Clark et al. (2005). Normal fault traces in black are slightly modified from Bateman (1965), Stone et al. (2000), and Du Bray and Moore (1985) (RV, MW, and MU transects, respectively); normal fault trace in blue is inferred based on AHe ages versus elevation graph (see Fig. 6) and geomorphology. Sample numbers corresponding for each age are in Table 1. Cross sections for each transect are shown in Figure 5.

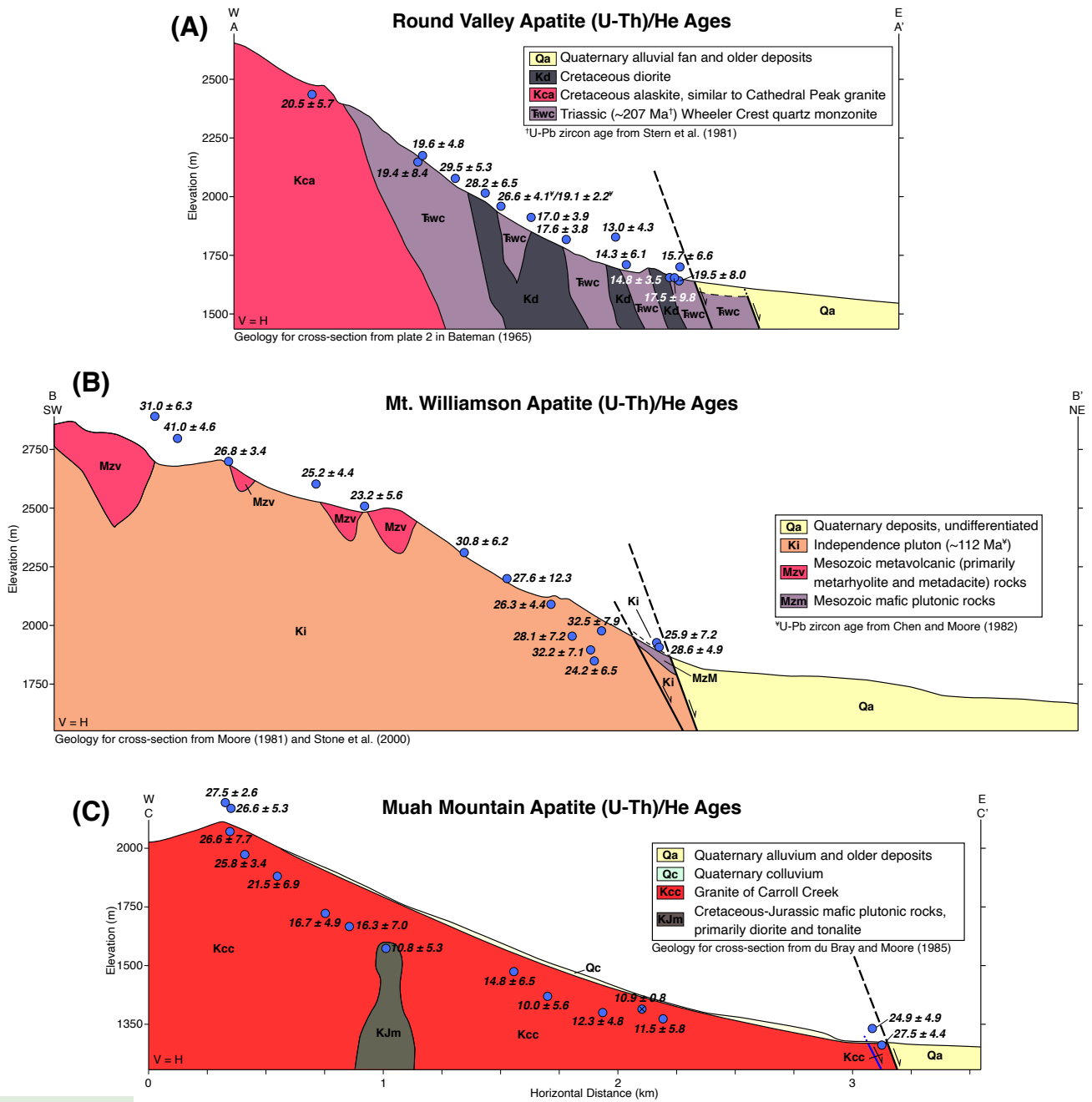

Figure 5. Apatite (U-Th)/He (AHe) ages projected onto interpretive cross sections along the Round Valley (A), Mount Williamson (B), and Muah Mountain (C) AHe transects (sample location with "x" on the blue circle is an AHe age from Clark et al., 2005). Normal fault trace in blue is inferred based on AHe ages versus elevation graph (see Fig. 6) and geomorphology. For locations of cross-section lines, see Figure 4.

unmapped normal fault slivers have been documented along the fault-bounded range flank of the White and Inyo mountains (Stockli et al., 2003; Lee et al., 2009). The absence of appropriate geologic markers makes it impossible to confirm the magnitude of this inferred offset; nevertheless, duplication of apatite fission-track data (e.g., Fitzgerald, 1992; Foster and Gleadow, 1996) and (U-Th)/He data (Stockli et al., 2003) have been used to estimate the magnitude of normal fault offset.

Interestingly, replicate analyses from the lowest elevation sample (#RV-1960-19) of these three samples yield two statistically distinct age groups—RV-1960a-19 and RV-1960b-19 (Tables 1 and S1 [footnote 1]) at 19.1 ± 2.2 Ma and 26.6 ± 4.1 Ma, respectively. While there is no obvious explanation in terms of He kinetic variation, such as radiation damage or composition and/or zoning (Th/U), the preservation of different age groups from a single sample from within the fault zone appears to indicate intra-sample heterogeneity or fluid alteration (e.g., Gorynski et al., 2014; Beltrando et al., 2015).

At MW, 12 samples collected from the Cretaceous Independence pluton (granite rocks) and three samples from Mesozoic metavolcanic rock (metarhyolite and metadacite) (Moore, 1981; Stone et al., 2000) over a vertical distance of 1043 m record AHe ages that range from ca. 23.2 Ma to ca. 41.0 Ma (Figs. 4B, 5B, and 6B). Fourteen of those samples, covering the entire vertical transect, yield ages that overlap, within error; these ages return a calculated elevation-invariant mean age of 28.1 ± 5.9 Ma (Fig. 6B). One MW sample yields an anomalous and over-dispersed mean age of ca. 41.0 Ma, an outlier relative to the 14 other samples. A number of factors may explain this outlier, such as the potential presence of U-Th–bearing mineral or fluid inclusions (Lippolt et al., 1994) or He implantation from U-Th–bearing minerals (Belton et al., 2004).

At MU, 15 AHe samples (including one from Clark et al., 2005) were collected from Cretaceous granite, diorite, and tonalite (Du Bray and Moore, 1985) that span a vertical distance of ~1040 m (Figs. 4C, 5, and 6C). Within error, the two lowest elevation samples record ages that are the same as the four highest elevation samples, implying that the two low-elevation samples record a minimum vertical offset of ~800 m and age duplication along a normal fault within the footwall of the SNNF (Figs. 5C and 6C). These six samples record an elevation-invariant mean age of 26.5 ± 2.0 Ma. The other eight samples, over a vertical distance of 501 m, yield ages that overlap, within error. These ages return a calculated elevation-invariant mean age of 12.9 ± 5.3 Ma. One sample falls within a PRZ between the two elevation-invariant trends (Fig. 6C).

Our MW and MU transects straddle two published vertical AHe transects in the footwall of the SNNF—one up the Mount Whitney Portal (MWP; ~8–9 km south of the MW transect) (House et al., 1997) and the other up the Horseshoe Meadow Road (HM; ~7 km north of the MU transect) (Clark et al., 2005) (Fig. 2). The vertical distance between samples from these two transects is typically 330–785 m and 97–409 m, respectively, and significantly larger than the vertical distance between all but two of our samples (typically ≲100 m). The MWP samples yield AHe ages that increase linearly from ca. 22.7 Ma at the range front (1985 m elevation) to ca. 74.6 Ma from near the top of Mount Whitney (4405 m elevation) (House et al., 1997) (Fig. 7). The HM AHe sample ages increase linearly from ca. 20.8 Ma (1666 m elevation) to ca. 52.2 Ma (2885 m elevation) (Clark et al., 2005) (Fig. 7). Clark et al.'s lowest elevation sample is located at the base of the MU transect; therefore, we included it as part of the MU transect (Figs. 6C and 7E).

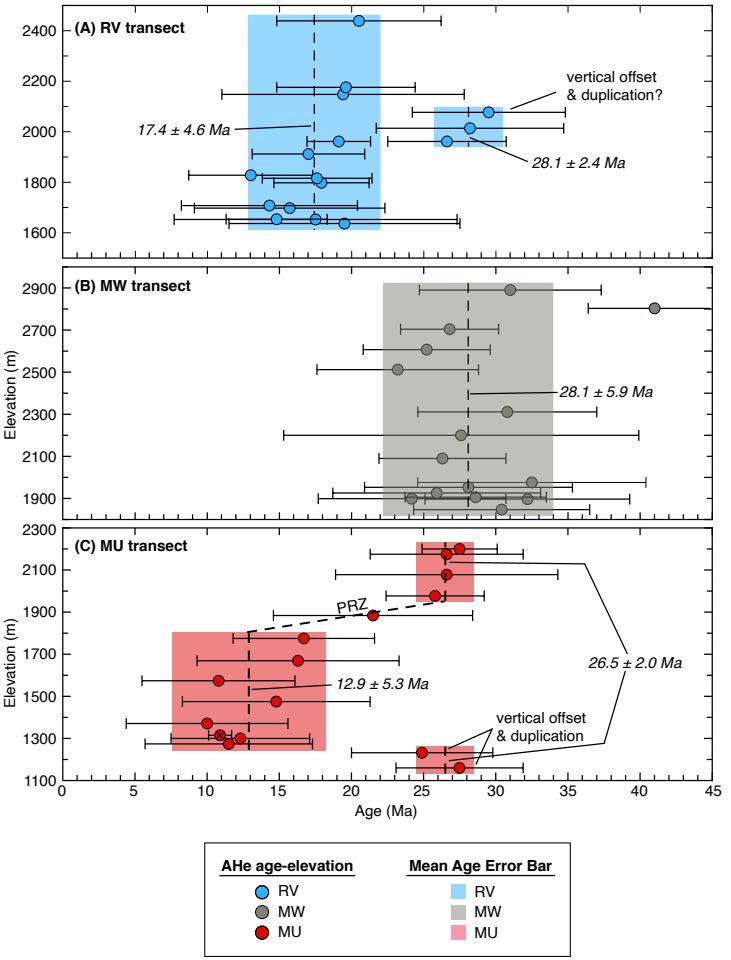

Figure 6. Plot of apatite (U-Th)/He (AHe) ages versus elevation showing the cooling histories for the southern Sierra Nevada normal fault footwall transects (A) Round Valley (RV), (B) Mount Williamson (MW), and (C) Muah Mountain (MU) (red circle with an "x" is an AHe age from Clark et al., 2005). Horizontal lines show 2σ error associated with each apatite age; dashed vertical line shows the mean age (in italic font) for elevation-invariant apatite ages; 50% transparent color bar shows the associated 2σ error for each elevation-invariant mean age; PRZ—partial retention zone.

TABLE 1. SUMMARY OF APATITE (U-Th)/He SAMPLE PARAMETERS AND MEAN AGES FOR SAMPLES COLLECTED IN THE FOOTWALL OF THE SOUTHERN SIERRA NEVADA RANGE FRONT NORMAL FAULT

Sample	Latitude*	Longitude*	Elevation (m)	Mean age (Ma)	±2σ	Replicates†
Round Valley transect						
RV-1634-19	37.45193	–118.63697	1637	19.5	8.0	7
RV-1650-13	37.44747	–118.63866	1653	17.5	9.8	3
RV-1654-18	37.44748	–118.63847	1654	14.8	3.5	11
RV-1700-19	37.43725	–118.64130	1698	15.7	6.6	6
RV-1710-19	37.45665	–118.63925	1708	14.3	6.1	15
RV-1797-19	37.42683	–118.64591	1798	17.9	3.3	7
RV-1816-19	37.45813	–118.64156	1816	17.6	3.8	7
RV-1827-19	37.44552	–118.64118	1828	13.0	4.3	6
RV-1912-19p	37.45864	–118.64298	1912	17.0	3.9	6
RV-1960a-19§	37.44589	–118.64602	1962	19.1	2.2	4
RV-1960b-19§	37.44589	–118.64602	1962	26.6	4.1	5
RV-2014-19	37.45925	–118.64485	2014	28.2	6.5	5
RV-2074-19	37.45933	–118.64609	2077	29.5	5.3	4
RV-2148-19	37.44603	–118.64953	2148	19.4	8.4	6
RV-2176-19	37.45921	–118.64752	2176	19.6	4.8	5
RV-2254-19	37.44742	–118.65381	2439	20.5	5.7	4
Mount Williamson transect						
MW-1848-19	36.69582	–118.24747	1847	30.4	6.1	9
MW-1897-19	36.65810	–118.23526	1897	32.2	7.1	10
MW-1899-19	36.65813	–118.23547	1899	24.2	6.5	9
MW-1904-19	36.67826	–118.24247	1906	28.6	4.9	5
MW-1925-19	36.67728	–118.24193	1926	25.9	7.2	6
MW-1953-18	36.64901	–118.23574	1953	28.1	7.2	8
MW-1996-19	36.67547	–118.24351	1976	32.5	7.9	12
MW-2089-19	36.67438	–118.24534	2090	26.3	4.4	6
MW-2202-19	36.67222	–118.24611	2200	27.6	12.3	11
MW-2310-19	36.67048	–118.24710	2311	30.8	6.2	8
MW-2512-19	36.66525	–118.24867	2512	23.2	5.6	6
MW-2607-19	36.66537	–118.25119	2607	25.2	4.4	4
MW-2704-19	36.66275	–118.25387	2704	26.8	3.4	7
MW-2800-19	36.65987	–118.25452	2803	41.0	4.6	5
MW-2892-19	36.65883	–118.25499	2890	31.0	6.3	6
Muah Mountain transect						
MU-1157-19#	36.44036	–118.04456	1160	27.5	4.4	5
MU-1232-19#	36.39460	–118.04020	1232	24.9	4.9	7
MU-1274-18	36.42583	–118.05340	1274	11.5	5.8	5
MU-1301-19	36.42948	–118.05630	1300	12.3	4.8	5
SN-LP-1a**	36.42680	–118.05510	1315	10.9	0.8	1
MU-1370-19	36.42871	–118.05874	1371	10.0	5.6	5
MU-1474-19	36.43050	–118.06035	1475	14.8	6.5	11
MU-1574-19	36.42650	–118.06597	1574	10.8	5.3	5
MU-1669-19	36.42475	–118.06754	1669	16.3	7.0	6
MU-1775-19	36.42330	–118.06856	1775	16.7	4.9	5
MU-1885-19	36.42098	–118.07061	1884	21.5	6.9	11
MU-1977-19	36.41970	–118.07202	1977	25.8	3.4	8
MU-2076-19	36.41781	–118.072602	2078	26.6	7.7	4
MU-2175-19	36.41529	–118.072449	2175	26.6	5.3	6
MU-2200-19	36.41485	–118.072669	2200	27.5	2.6	6

*World Geodetic System 1984 datum.
†Number of replicates per sample. See Table S1 (text footnote 1) for replicate analyses.
§Replicate analyses from sample RV-1960-19 yield two statistically distinct populations, RV-1960a-19 and RV-1960b-19 (see Table S1 [text footnote 1]).
#Sample located in a hanging-wall block of a normal fault located in the footwall of the southern Sierra Nevada normal fault (SNNF), thus recording vertical offset and duplication.
**From Clark et al. (2005); error in age is standard error.

Figure 7 is interactive. Graph, labels, and data sets for this figure are organized in a series of layers that may be viewed separately or in combination using the capabilities of the Acrobat (PDF) layering function (click "Layers" icon along vertical bar on left side of window for display of available layers, and/or turn layers on or off by clicking the box that encompasses the layer label located within the gray box beneath the plot). To interact with Figure 7 if reading the full-text version of this paper, please visit https://doi.org/10.1130/GEOS.S.22662076.

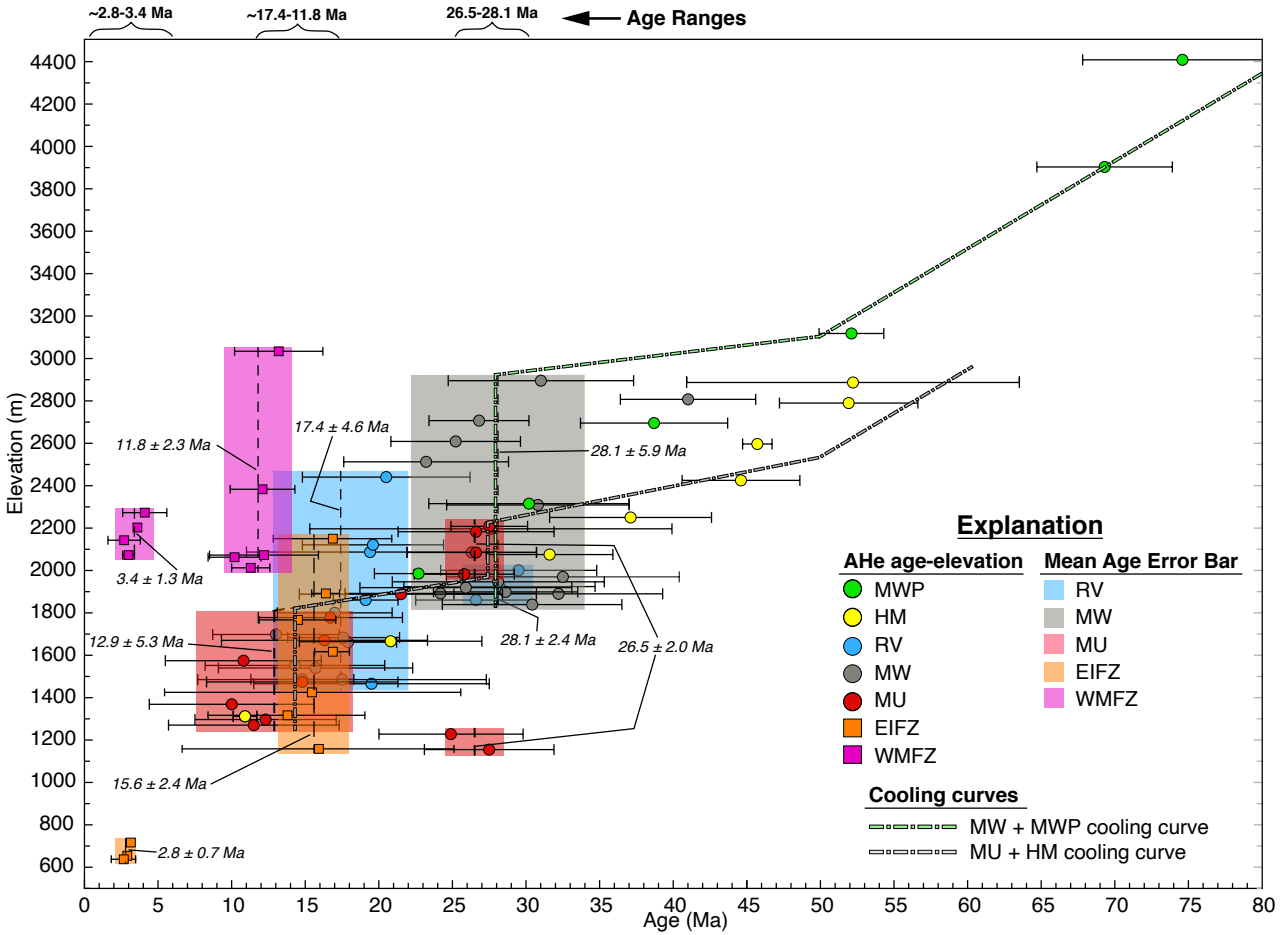

Layers

- A. Apatite (U-Th)/He age vs. Elevation graph
- B. AHe age vs Elevation data from transect RV
- C. AHe age vs Elevation data from transect MW
- D. AHe age vs Elevation data from transect MU
- E. AHe age vs Elevation data from transect EIFZ
- F. AHe age vs Elevation data from transect WMFZ
- G. AHe age vs Elevation data from transect MWP
- H. AHe age vs Elevation data from transect HM
- I. Interpretative cooling curve for MWP & MW
- J. Interpretative cooling curve for HM & MU

Figure 7 (interactive). A composite plot showing apatite (U-Th)/He (AHe) ages versus elevation (layer A) from our transects Round Valley (RV) (layer B), Mount Williamson (MW) (layer C), and Muah Mountain (MU) (layer D) in the footwall of the southern Sierra Nevada normal fault (SNNF), from transects from the footwall to the Eastern Inyo fault zone (EIFZ) (Lee et al., 2009) (layer E), to the White Mountains fault zone (WMFZ) (Stockli et al., 2003) (layer F), in the Mount Whitney Portal (MWP) (House et al., 1997) (layer G), up the Horseshoe Meadow Road (HM) (Clark et al., 2005) (layer H), and interpreted cooling histories of combined MWP and MW data (layer I) and combined HM and MU data (layer J). Also shown are the age ranges for elevation-invariant samples across sampling transects. Horizontal lines show 2σ error associated with each apatite age; dashed vertical line shows the mean age (in italic font) for elevation-invariant apatite ages; 50% transparent color bar shows the associated 2σ error for each elevation-invariant mean age. Graph, labels, and data sets for this figure are organized in a series of layers that may be viewed separately or in combination using the capabilities of the Acrobat (PDF) layering function (click "Layers" icon along vertical bar on left side of window for display of available layers, and/or turn layers on or off by clicking the box that encompasses the layer label located within the gray box beneath the plot). To interact with Figure 7 if reading the full-text version of this paper, please visit https://doi.org/10.1130/GEOS.S.22662076.

Interpretation of Apatite (U-Th)/He Ages

Our new apatite (U-Th)/He ages from the three transects yield two distinct elevation-invariant age arrays, with sample mean ages overlapping within error. These two AHe age clusters indicate two episodes of cooling (Figs. 7B, 7C, and 7D), which we interpret as recording two distinct periods of exhumation and rapid normal fault slip along the SNNF: (1) initiation of major exhumation and normal fault slip along the length of the SNNF at ca. 28.1–26.5 Ma (mean age ± 2σ of 27.7 ± 5.0 Ma) and (2) a second episode of normal fault slip along the SNNF, recorded in the RV and MU transects, but not the MW transect, at ca. 17.4–12.9 Ma (mean age ± 2σ of 15.7 ± 6.5 Ma). Diachronous normal fault-slip histories along the SNNF during the middle Miocene, whereby the RV segment recorded slip at ca. 17.4 Ma and the MU segment recorded slip at ca. 12.9 Ma, are viable alternative interpretations of the elevation-invariant middle Miocene AHe ages (Figs. 7B and 7D). We postulate that the second, younger pulse of middle Miocene normal fault slip is not observed in the MW samples as lower portions of the footwall along this section of the eastern Sierra Nevada range front, which might record the middle Miocene cooling and exhumation event, were not exhumed due to insufficient fault slip and/or are buried by the most areally extensive alluvial fan deposits along the SNNF (Fig. 2).

In contrast to the two discreet cooling events observed in our AHe MW and MU transects (Figs. 6 and 7), which we interpret as recording footwall exhumation and fault slip, AHe samples from the nearby MWP and the HM transects yielded ages that increase linearly with elevation (Fig. 7). This pattern indicates slow cooling and has been interpreted as recording erosion (0.04–0.06 mm/yr) (House et al., 1997; Clark et al., 2005) (Fig. 7). We suggest that a few key observations and comparisons between our AHe transects and the MWP and HM AHe transects resolve this apparent contradiction in interpretations. First, a comparison of AHe versus elevation data between MW and MWP, and between MU and HM, shows two important geometric relations: (1) MW and MU data clearly fall off the linear relationship observed in the MWP and HM data. More specifically, MW and MU transects include high-elevation samples with ages older than the projected erosion lines. (2) The elevation difference between samples is significantly larger for the MWP and HM transects compared to samples from the MW and MU transects (cf. Figs. 7C and 7G and Figs. 7D and 7H). The elevation difference is ≥170 m to as much as 785 m between all but two MWP and HM samples, whereas the elevation difference is ≤114 m between all but two MW and MU samples. Thus, the higher-density samples in the MW and MU transects fill in the elevation "gaps" among the lower-density, low-elevation samples of the MWP and HM transects. A consequence of this relation is that the (i) two low-elevation MWP samples fall within the MW rapid cooling event, and (ii) three low-elevation HM samples (including the lowest elevation sample at the base of the MU transect) fall within one or the other of the two rapid MU cooling events. Second, in Figures 7I and 7J, we show potential cooling curves of the AHe data from the MW, MU, MWP, and HM transects that incorporate both slow cooling (erosion) and rapid cooling (fault slip). A slow cooling curve during the late Cretaceous to early Oligocene fits the older higher-elevation ages from the MWP and HM transects and rapid cooling curves, one during the late Oligocene and the other during the middle Miocene, fit the MW and MU transects, as well as the younger low-elevation ages from the MWP and HM transects. Third, the significant (~24°) westward tilting of the Inyo Mountains during middle Miocene slip along the east-dipping Eastern Inyo fault zone (EIFZ) (Lee et al., 2009) (Figs. 1 and 2) must be accommodated to the west; middle Miocene slip along the length of the SNNF between the RV to MU transects provides a simple mechanism for accommodating this tilt.

Comparing our new multi-stage SNNF normal fault-slip history to the normal fault-slip histories on the range-bounding faults in ranges east-adjacent to the southern Sierra Nevada, the east-dipping EIFZ bounding the eastern flank of the Inyo Mountains and the west-dipping White Mountains fault zone (WMFZ) bounding the western flank of the White Mountains (Fig. 1A), shows diachronous and overlapping Cenozoic normal fault-slip histories in this part of the western edge of the Basin and Range (Fig. 7). While the oldest range-bounding normal fault slip at 27.7 ± 5.0 Ma is recorded only along the SNNF, the younger and dominant episode of slip along range bounding normal faults occurred synchronously during the middle Miocene. The middle Miocene period of slip is recorded as a second episode of fault slip along the RV and MU segments of the SNNF at 15.7 ± 6.5 Ma but as the onset of normal fault slip along the EIFZ and the WMFZ at ca. 15.6–11.8 Ma (Stockli et al., 2000, 2003; Lee et al., 2009) (Fig. 7). Given that the elevation-invariant age trends along the RV, MU, EIFZ, and WMFZ yield the same age, within error, the four areas recorded synchronous normal fault slip at the same time of 14.4 ± 5.1 Ma (mean age ±2σ). The EIFZ and WMFZ samples also yield AHe ages that record a pulse of normal fault slip at ca. 3.1 Ma (Figs. 7F and 7G) linked to transtensional fault-slip deformation within the Walker Lane (Stockli et al., 2000; Lee et al., 2009). Preliminary landscape evolution modeling hints that at least the MU transect also records a Pliocene episode of normal slip (Lee et al., 2021).

If our interpretation that the southern Sierra Nevada escarpment developed since the onset of normal fault slip along the SNNF in the late Oligocene, we can place constraints on the magnitude of fault slip, fault-slip rates, and rate of horizontal extension along the SNNF since the late Oligocene–early Miocene (34.0–22.2 Ma). Given the elevations of Round Valley Peak, Mount Williamson, and Muah Mountain, the highest point in the footwalls of the RV, MW, and MU transects, depth to basement estimates based on gravity in the hanging wall of each transect (Saltus and Jachens, 1995), a fault dip of 70 ± 10° (Fig. 3), and the age of the late Oligocene elevation invariant trend for each of the transects (Fig. 6), we calculate minimum values for long-term magnitude of fault slip, fault-slip rates, and rate of horizontal extension, at each of the three transects (Table 2). For RV, MW, and MU, the minimum vertical offset, or throw, across the SNNF at each location is 6.6–7.6, 8.4–9.4, and 10.4–11.4 km, which based on the age of onset of normal slip, yields a vertical throw rate of 0.2–0.3, 0.2–0.4, and 0.4–0.5 mm/yr and downdip rate of 0.2–0.3, 0.3–0.5, and 0.4–0.5 mm/yr, respectively, since the late Oligocene (Table 2). The calculated

TABLE 2. CALCULATED MINIMUM SLIP RATES AT THE THREE AHe VERTICAL TRANSECTS FROM THE SOUTHERN SIERRA NEVADA NORMAL FAULT

Transect	Peak elevation (km)*	Depth to basement (km)†	Minimum vertical offset (km)	Age (Ma)§	#Vertical slip rate (mm/yr)	#Downdip fault-slip rate (mm/yr)	#Horizontal extension rate (mm/yr)
RV	3.6	3–4	6.6–7.6	28.1 ± 2.4	0.2–0.3	0.2–0.3	<0.1–0.2
MW	4.4	4–5	8.4–9.4	28.1 ± 5.9	0.2–0.4	0.3–0.5	<0.1–0.2
MU	3.4	7–8	10.4–11.4	26.5 ± 2.0	0.4–0.5	0.4–0.5	0.1–0.3

Note: RV—Round Valley Peak; MW—Mount Williamson; MU—Muah Mountain.
*Peak elevations are from the highest peak—RV, MW, and MU—located in the footwall of each transect.
†Depth to basement values are from Saltus and Jachens (1995).
§Age is the late Oligocene elevation-invariant age (see Fig. 6).
#Calculated minimum slip rates are based on a fault dip of 70 ± 10° (see text Fig. 3).

horizontal extension rates are <0.1–0.2, <0.1–0.2, and 0.1–0.3, respectively, since the late Oligocene. For comparison, our calculated long-term (10^7 yr) average horizontal extension rate (<0.1–0.3 mm/yr) along the SNNF is the same as, to ~1.5× higher, than the late Pleistocene to Holocene horizontal extension rate of <0.1–0.2 mm/yr (based on a fault dip of 70° +13/–15°) along an ~40-km-long section of the SNNF that straddles the Mount Williamson range front (Le et al., 2007). Our calculated long-term vertical slip rates along the SNNF are less than the middle Miocene vertical slip rates along the east-dipping EIFZ (≥1.9 mm/yr) (Lee et al., 2009), and less than to similar to the vertical slip rate along the west-dipping WMFZ (Stockli et al., 2003) (~0.5 mm/yr; vertical rate recalculated using the nominal closure temperature of ~55 °C for AHe; Flowers et al., 2009).

DISCUSSION

Diachronous Initiation of Normal Fault Slip along the Length of the Sierra Nevada Frontal Fault System

Although the Sierra Nevada is a rigid continental block (e.g., Wright, 1976; Dixon et al., 2000), normal fault slip along the ~600-km-long Sierra Nevada frontal fault system, which defines the eastern boundary of this block, did not initiate simultaneously. Our interpretation of AHe data from our three transects shows that the onset of normal fault slip along most of the SNNF, which extends along strike along the southern half of the Sierra Nevada for ~130 km, initiated during the late Oligocene. The timing of initiation of normal fault slip is younger along the southernmost part of the SNNF and along the northern part of the Sierra frontal fault system. At the southern end of the Sierra Nevada, located along the southernmost exposures of the SNNF near the intersection with the Garlock fault, Loomis and Burbank (1988) documented that Sierran-derived sandstones, gravels, and boulders were first deposited in the El Paso basin (Fig. 1G-*i*; italicized roman numbers in red stars in layer G of Fig. 1 show location of study areas) at ca. 8 Ma, implying that the SNNF was active at this time. About 40 km to the north, in the Indian Wells Valley region (Fig. 1G-*ii*), seismic-reflection, drill-hole, sedimentological, and $^{40}Ar/^{39}Ar$ and (U-Th)/He data were used by Kamola et al. (2005) to suggest that normal slip along this segment of the SNNF initiated during the late Miocene.

To the north of our study area, in the central Sierra Nevada across the Sonora Pass region (Fig. 1G-*iii*), slip along range-front normal faults initiated after emplacement of the top of the Relief Peak Formation and was ongoing during emplacement of the Table Mountain latite, indicating normal faulting initiated at ca. 10.4 Ma (our interpretation based on geology from Busby et al., 2013 and geochronology from Koerner et al., 2009 and Pluhar et al., 2009). Farther north, apatite fission-track, geophysical, and geologic data from the Carson Range (Fig. 1G-*iv*), which defines the eastern edge of the Sierra Nevada at ~39° latitude, indicates that significant slip began at <10 Ma, with most of the extension accumulating since 5 Ma (Surpless et al., 2002). Farther north, at the approximate latitude of Reno, Nevada (Fig. 1G-*v*), Henry and Perkins (2001) showed that extension along the range front developed in two stages, an initial phase at ca. 12 Ma and a younger, larger-magnitude event at ca. 3 Ma that resulted in the modern structural and topographic boundary. At the northern end of the Sierra Nevada (Fig. 1G-*vi*), the 16 Ma Lovejoy basalt and ca. 5 Ma Mehrten Formation are offset by the same amount, 600–1000 m, across the Sierra Nevada frontal fault system, indicating that normal fault slip began after ca. 5 Ma (Wakabayashi and Sawyer, 2001).

The diachronous fault-slip history along the Sierra Nevada frontal fault system also appears to be recorded in crest elevations and bedrock fault scarp height. The SNNF is located at the base of the highest elevations along the Sierra Nevada crest. At Mount Williamson, the highest elevation among our three transects, the height of the footwall escarpment above the valley floor (Owens River) is ~3.25 km. Crest elevations in the footwall of the Sierra Nevada frontal fault system and bedrock fault scarp height decrease to the south and north of the SNNF (see fig. 3 in Wakabayashi and Sawyer, 2001). These observations are consistent with the longer slip history along the SNNF versus the Sierra Nevada frontal fault system to the south and north, assuming similar long-term fault-slip rates along the length of the fault system.

Cenozoic Uplift of the Sierra Nevada

One of the long-standing disagreements about the evolution of the Sierra Nevada is its uplift history. Many researchers have argued for late Mesozoic–early Cenozoic uplift of the Sierra Nevada followed by either no change or a decrease in elevation throughout the Cenozoic (e.g., Wernicke et al., 1996; Wolfe et al., 1997; House et al., 1998, 2001; Poage and Chamberlain, 2002; Cecil et al., 2006; Mulch et al., 2006; Cassel et al., 2009, 2012b). In contrast, others have argued that the Sierra Nevada was uplifted in the late Mesozoic, decreased in elevation during the middle Cenozoic, and then was uplifted a second time during the late Cenozoic (e.g., Lindgren, 1911; Axelrod, 1957; Huber, 1981; Loomis and Burbank, 1988; Unruh, 1991; Christensen, 1996; Wakabayashi and Sawyer, 2001; Stock et al., 2004; Clark et al., 2005; Pelletier, 2007; McPhillips and Brandon, 2012; Wakabayashi, 2013). Some of those who espouse the latter view made predictions about the timing of the second episode of uplift. For example, Clark et al. (2005) combined geomorphology and AHe data from the southern Sierra Nevada to argue that this part of the range reached 1.5 km in elevation by the late Cretaceous followed by two additional uplift events, one between 32 Ma and 3.5 Ma and another ≤3.5 Ma, which increased the elevation to the 4 km of today. Pelletier (2007) applied two different numerical models of bedrock channel erosion, a sediment-flux–driven model and a stream power model, to the southern Sierra Nevada. The results from the sediment-flux model showed a 1 km pulse of uplift at ca. 60 Ma and a second ~0.5 km pulse of uplift at ca. 10 Ma and from the stream power model a 1 km pulse of uplift at ca. 30 Ma and an ~0.5 km pulse at ca. 10 Ma. Results from the coupled thermal-kinematic model Pecube, applied to published low-temperature thermochronometric data from the southern Sierra Nevada, show that this part of the Sierra Nevada recorded an uplift history in the late Mesozoic, followed by a reduction in surface elevation, and then renewed surface uplift between 30 and 10 Ma (McPhillips and Brandon, 2012). Our AHe results from the eastern escarpment of the southern Sierra Nevada yield histories of cooling, exhumation, and normal fault slip along the SNNF at ca. 28–27 Ma and ca. 17–13 Ma, which are broadly consistent with postulated late Cenozoic uplift of the Sierra Nevada.

In two-dimensional models of crust "floating" in a ductile or inviscid lower crust and dislocations in an elastic half-space, slip along normal faults in the crust, and the associated unloading of the footwall, results in uplift of the normal-faulted footwall and subsidence of its hanging wall (e.g., Vening Meinesz, 1950; Buck, 1988; Wernicke and Axen, 1988; King and Ellis, 1990; Egan, 1992; Thompson and Parsons, 2009; Martel et al., 2014). In Thompson and Parsons' (2009) model for slip along the Sierra Nevada frontal fault system, normal fault slip of 4 km resulted in 1.3 km of uplift of the Sierra Nevada footwall. Martel et al.'s (2014) models for the Sierra Nevada frontal fault system yielded footwall uplift of hundreds of meters to as much as 1 km in the region of our MW transect. Our interpretation that the AHe data record two episodes of normal fault slip indicate that the southern Sierra Nevada likely experienced at least few hundred meters of uplift during the late Oligocene and again in the middle Miocene, although our structural and AHe data do not permit us to directly assess the magnitude of the uplift.

Timing of Normal Faulting across the Basin and Range

Our interpretation of two episodes of normal fault slip along the SNNF, the oldest during the late Oligocene and the younger during the middle Miocene, are also recorded across the Basin and Range. However, the evidence for an episode of late Oligocene normal faulting in the Basin and Range is scarce, whereas evidence for an episode of middle Miocene normal faulting is extensive. Across the Basin and Range, normal fault slip similar in age to the ca. 27 Ma initiation age along the SNNF is local and generally of low magnitude (Fig. 1H-*a*; lower case italicized letters in green diamonds in layer H of Fig. 1 show location of study areas that record late Oligocene–early Miocene normal fault slip) (Table 3). Within the northern Wassuk Range, western Nevada, local normal and strike-slip faulting occurred at ca. 27–25 Ma and at 23–22 Ma (Dilles and Gans, 1995) (Fig. 1H-*b*). Local and minor normal faulting in western Nevada of this age is consistent with field observations that tuff-filled paleovalleys as young as ca. 23 Ma flowed westward from central Nevada across western Nevada and the northern Sierra Nevada into the Great Valley, which implies that any Oligocene-age normal faulting did not result in significant topographic relief that would have disturbed westward flowing river channels (Henry et al., 2012) (Fig. 1E). In central Nevada, within the Tobin Range, a minor phase of normal faulting initiated during the early Oligocene (Gonsior and Dilles, 2008) (Fig. 1H-c). In east-central Nevada, normal faulting initiated during the late Oligocene–early Miocene in the Grant Range and accommodated ~24 km extension (~115%) (Long and Walker, 2015; Long et al., 2018) (Fig. 1H-*d*). The maximum age of normal faulting at the northern end of the northern Snake Range is 24.0 ± 1.3 Ma (K/Ar on sanidine) (Gans et al., 1989) (Fig. 1H-*e*), indicating that normal faulting here may be as old as latest Oligocene. In the eastern Pinon Range and central Huntington Valley, and the Ruby Mountains–East Humbolt Range region of northeastern Nevada, minor extension occurred between ca. 31.1 and 24.4 Ma and ca. 25–21 Ma, respectively (Lund Snee et al., 2016; McGrew and Metcalf, 2021) (Fig. 1H-*f*).

In contrast, evidence for large-magnitude normal faulting of middle Miocene age is regionally extensive across the Basin and Range (Fig. 1I; numbers in light-blue ovals in layer I of Fig. 1 show the location of study areas that record middle Miocene normal fault slip and are tied to Table 3). Evidence for middle Miocene normal faulting extends along most of the length of the Sierra Nevada frontal fault system; covers eastern California east of the southern Sierra Nevada and north of the Garlock fault; encompasses western, central, and eastern Nevada; includes southeastern Nevada–northwestern Arizona; and reaches as far east as the Wasatch Range front, the eastern boundary of the Basin and Range Province. The ample evidence for normal faulting of middle Miocene age across the Basin and Range, from its western boundary along the Sierra Nevada frontal fault system to its eastern boundary along the Wasatch range front fault, suggests that this was a period of major east-west extension.

Our AHe data indicating late Oligocene and middle Miocene normal slip along the SNNF, combined with data showing that the SNNF is active today (Berry, 1997; Le et al., 2007) and the numerous studies documenting middle

TABLE 3. LATE OLIGOCENE–EARLY MIOCENE NORMAL FAULTING AND ONSET OF AND/OR MAJOR EPISODE OF MIDDLE MIOCENE NORMAL FAULTING, BASIN AND RANGE

Range	Location #*	Initiation age (Ma)	Reference
Late Oligocene–Early Miocene			
Southern Sierra Nevada, CA	a	Ca. 28.5–26.5	This study†
Northern Wassuk Range, NV	b	Ca. 26–25	Dilles and Gans, 1995§
Tobin Range, NV	c	Ca. 33	Gonsior and Dilles, 2008§
Grant Range, NV	d	Ca. 32–29; <28–31 to >15–19	Long and Walker, 2015; Long et al., 2018§
Northern Snake Range, NV	e	≤24.0 ± 1.3	Gans et al., 1989§
Huntington Valley-Pinon Range, NV	f	Ca. 31.1–24.4	Lund Snee et al., 2016§
Ruby Mountains-East Humbolt Range, NV	f	Ca. 25–21	McGrew and Metcalf, 2021#
Middle Miocene			
Beaver Dam Mountains, UT	1	Ca. 16	Stockli, 1999†
Black Mountains, CA	2	Ca. 12	Bidgoli et al., 2015†
Black Mountains, NV	3	15.6–15.8	Faulds et al., 1995§
Cerbat Mountains, NV	4	Ca. 16.6	Faulds et al., 2010§
Canyon Range, UT	5	Ca. 19–15	Stockli et al., 2001†
East Range, NV	6	Ca. 17–15	Fosdick and Colgan, 2008; Johnstone and Colgan, 2018†
Gardnerville Basin, NV	7	Middle Miocene(?)	Cashman et al., 2009§
Gold Butte block, NV	8	Ca. 17	Beard, 1996; Fitzgerald et al., 1991; Reiners et al., 2000†,§
Highland Range, NV	9	16.2 ± 0.2	Faulds et al., 2002§
Inyo Mountains, CA	10	15 ± 2.4	Lee et al., 2009†
Mina Deflection, CA-NV	11	>12 and ca. 12–3.8	Tincher and Stockli, 2009; McCosby, 2019§
Northern Newberry Mountains, NV	12	Ca. 16.2	Ruppert et al., 1999§
Panamint Range, CA	13	Ca. 10	Bidgoli et al., 2015†
Paradise Range, NV	14	22–19	John et al., 1989§
Pine Forest Range, NV	Off map	12–11	Colgan et al., 2006; Johnstone and Colgan, 2018†
Southern Ruby Mountains, NV	15	17–15 to 12–10	Colgan et al., 2010†§
San Antonio Mountains, NV	16	24.0–16.8	Shaver and McWilliams, 1987; John et al, 1989§
Shoshone Range, NV	17	17–16	Colgan et al., 2008§
Southern Sierra Nevada, CA	18	Ca. 17–13	This study†
Silver Peak Range, NV	19	Ca. 12–8	Oldow et al., 2009§
Singatse Range, NV	20	Ca. 15–13	Proffett, 1977; Dilles and Gans, 1995; Surpless et al., 2002; Stockli et al., 2002†,§
Slate Range, CA	21	Ca. 14	Walker et al., 2014†
Northern Stillwater Range, NV	22	Ca. 14	MacNamee, 2015†
Southern Stillwater Range, NV	23	Ca. 18–14	Colgan et al., 2020†
Snake Range-Deep Creek Range, NV-UT	24	Ca. 18–16.5	Miller et al., 1999; Evans et al., 2015†
Tobin Range, NV	25	20(?)–14	Gonsoir and Dilles, 2008§
Toiyabe Range, NV	26	Ca. 15	Stockli, 1999†
Verdi Basin, CA-NV	27	Ca. 12	Henry and Perkins, 2001§
Central Wasatch Mountains, UT	28	12 ± 2	Armstrong et al., 2003; Ehlers et al, 2003†
Wassuk Range, NV	29	Ca. 15	Surpless et al., 2002; Gorynski et al., 2013†,§
Northern White Mountains, CA	30	11.8 ± 2.3	Stockli et al, 2003†,§

Note: CA–California; NV–Nevada; UT–Utah.
*For location of study areas, see alphanumeric labeled diamonds and ellipses in text Figure 1.
†Age constraints are from low-temperature thermochronology (zircon and/or apatite fission track, zircon and/or apatite (U-Th)/He, and/or apatite $^{4}He/^{3}He$ analyses) of footwall rocks.
§Age constraints are from $^{40}Ar/^{39}Ar$ or K/Ar geochronology on offset and tilted volcanic rocks, and/or detrital zircon analyses on offset and tilted sedimentary rocks.
#Geochronologic or thermochronologic technique not reported.

Miocene normal fault slip across the Basin and Range, indicate that the SNNF has been long-lived and has defined the stable western limit, or western breakaway zone, for the Basin and Range since the late Oligocene. Unlike the long-lived stable southern Sierra Nevada escarpment, normal faulting appears to have progressively encroached westward into the northern Sierra Nevada (latitudes of ~39°–40°), during the late Miocene–Pliocene (e.g., Surpless et al., 2002; Wakabayashi, 2013). Slip along the long-lived, east-dipping breakaway SNNF also accommodated the significant (~24°) westward tilting of the Inyo Mountains during the middle Miocene (Lee et al., 2009), which sits in the hanging wall of the SNNF (Fig. 1).

Implications for Geodynamic Processes Driving Normal Faulting along the Sierra Nevada Fault System

Prior to this detailed study, the uncertainty of the exact timing of late Cenozoic normal slip along the SNNF led to different combinations of crustal structure and geodynamic processes hypothesized as drivers for slip along the frontal normal fault system. Our documented slip history along the SNNF, combined with the published normal fault-slip histories across the Basin and Range, provide a framework to test these hypotheses.

One early hypothesis was the development of a slab window. In this postulate, asthenosphere infilled the vacated space as the subducted Farallon slab was removed in the wake of the northward-migrating Mendocino triple junction (e.g., Crough and Thompson, 1977; Best and Hamblin, 1978; Dickinson and Snyder, 1979; Atwater and Stock, 1998; Zandt and Humphreys, 2008). If slip along the Sierra Nevada frontal fault system was driven by this geodynamic process (e.g., Wakabayashi, 2013), then as the Mendocino triple junction migrated northward, one prediction is that the initiation age of fault slip should decrease northward from ca. 20 Ma in the southern Sierra Nevada at the latitude of ~35.3° (present-day latitude) to ca. 4–0 Ma at the latitude of ~40.5° (Fig. 1J). Our interpretation of AHe age results shows that this prediction is not viable: (1) because normal faulting along the SNNF is considerably older, in part, than the age of the Mendocino triple junction (ca. 15.1–10.9 Ma) at the locations of our transects, and (2) the slip history along the SNNF does not record an initiation age that decreases northward (Fig. 6).

In the Pacific–North American plate reconstructions of Atwater and Stock (1998), the rate of transtensional relative plate motion between the Pacific and North American plates increased by ~1.5 times during the middle Miocene. Thus, this rate increase in plate motion and partitioning of transtensional slip along the Pacific–North American plate boundary into an extensional component along the SNNF and to the east, and a transform component along Pacific–North American plate boundary provides a potential driver for the middle Miocene episode of normal slip across the Basin and Range (e.g., Colgan et al., 2006; Colgan and Henry, 2009), and by implication, the SNNF. In contrast to Atwater and Stock's (1998) reconstructions, DeMets and Merkouriev's (2016) higher-resolution Pacific–North American plate reconstructions show that during the past ~20 m.y., the slip direction between the two plates progressively rotated clockwise, suggesting a progressively increasing transform slip component along the plate boundary. Given the higher-resolution Pacific–North American plate reconstructions, we conclude that it is unlikely that transtensional motion along the Pacific–North American plate boundary was the sole driver for middle Miocene normal slip along the SNNF and extension across the Basin and Range to the east. Furthermore, as the Pacific plate did not contact the North American plate until ca. 28 Ma (Atwater and Stock, 1998), transtensional slip along this developing plate boundary does not explain late Oligocene onset of normal slip along the SNNF and across the few localities to the north and northeast within the Basin and Range that also record late Oligocene normal faulting (Figs. 1H and 1J).

A third postulate is a flexural-isostatic model of the lithospheric response to high rates of erosion in the high Sierra and deposition in the Great Valley during the past ~10 m.y. (Montgomery, 1994; Small and Anderson, 1995). This model shows that geomorphic forcing accounts for 100%–40% (versus 0%–60% tectonic forcing, including slip along the Sierra Nevada frontal fault system) of the differential rock uplift recorded in tilted sediments in the Sierra Nevada. In this model, if tectonic forcing contributes to uplift, then late Miocene slip should be recorded along the SNNF. Our AHe results yield an older episode of normal fault slip, indicating that this mechanism unlikely drove normal slip along the SNNF.

A fourth idea envisioned that during the Pliocene, foundering dense lithosphere mantle beneath the southern Sierra Nevada was replaced with upwelling asthenosphere (e.g., Ducea and Saleeby, 1996; Liu and Shen, 1998; Manley et al., 2000; Farmer et al., 2002; Saleeby et al., 2003; Jones et al., 2004; Zandt et al., 2004). In this hypothesis, the asthenosphere heated the lithosphere resulting in a decrease in lithosphere density and strength, an increase in its buoyancy, and an increase in gravitational potential energy. An increase in gravitational potential energy resulted in mean surface elevation uplift and increased extensional strain rates within an ~50 km distance east of the Sierra Nevada. AHe data indicate Pliocene normal slip along the EIFZ (Lee et al., 2009) and WMFZ (Stockli et al., 2003) (Figs. 7E and 7F), and preliminary landscape evolution modeling suggests a Pliocene episode of normal fault slip along the MU segment of the SNNF (Lee et al., 2021), consistent with this hypothesis. Although this geodynamic process cannot explain the initiation of normal fault slip along the SNNF during late Oligocene, the early stages of foundering (ca. 10 Ma; Ducea and Saleeby, 1998a, 1998b), may have been a contributing factor to driving the middle to late Miocene episode of normal slip along the MU transect of the SNNF and the WMFZ (Fig. 7).

The predominant tectonic model, which provides a geodynamic explanation for the onset of the major episode of extension across the Basin and Range during the middle Miocene, suggests that a combination of lithospheric buoyancy forces (gravitational potential energy) and plate boundary processes drove extension (e.g., Sonder and Jones, 1999; Dickinson, 2002; Colgan and Henry, 2009). In this postulate, high gravitational potential energy, hypothesized to be a consequence of: (1) thickened crust and high elevations following

Mesozoic contraction (e.g., Coney and Harms, 1984; Jones et al., 1998; DeCelles, 2004); (2) hot, buoyant asthenosphere that replaced the Farallon slab that steepened and fell away (e.g., Armstrong and Ward, 1991; Humphreys, 1995; Sonder and Jones, 1999; Humphreys, 2009; Schmandt and Humphreys, 2011); and (3) the emplacement of the Yellowstone hotspot (e.g., Parsons et al., 1994; Saltus and Thompson, 1995; Camp et al., 2015), which primed the future Basin and Range for extension. During the middle Miocene, the combination of foundering of the last vestige of the Farallon slab (Armstrong and Ward, 1991; Humphreys, 1995) and trench retreat (slab rollback) along the Juan de Fuca–North American subduction zone allowed the pre-conditioned Basin and Range crust to collapse and extend from the SNNF on the west to the Wasatch fault on the east, westward in the wake of that retreat (e.g., Colgan and Henry, 2009; Lee et al., 2020). Normal fault slip along the SNNF was not explicitly included in this hypothesis but was implied.

The view that overthickened crust and high elevations following Mesozoic contractional deformation was a critical condition for middle Miocene extension has been recently challenged by Lund Snee and Miller (2022). Lund Snee and Miller's (2022) alternative hypothesis, which builds upon the hypotheses of Humphreys (1995) and Sonder and Jones (1999), is that the hot, thermally weak continental lithosphere and high elevations were the consequence of two processes: (1) as others have postulated, replacement of the steepening and southward-migrating northern edge of the Farallon slab with hot and buoyant asthenosphere and (2) the subsequent substantial input of heat, associated with the addition of magma into the lithosphere, which drove the ignimbrite flareup, thermally weakened the crust, and increased its elevation (i.e., increased the gravitational potential energy). In this postulate, topographic uplift across the Basin and Range developed diachronously in response to the southward-migrating Farallon slab and the concomitant ignimbrite flareup. These changes to the continental lithosphere primed the proto–Basin and Range for extension. As others have also observed (e.g., Colgan and Henry, 2009; Camp et al., 2015), Lund Snee and Miller (2022) noted the temporal overlap of middle Miocene extension across the Basin and Range with final removal of the Farallon slab (Armstrong and Ward, 1991; Humphreys, 1995, 2009; Schmandt and Humphreys, 2011), the development of a gap in the Farallon slab and emplacement of the Yellowstone hotspot (e.g., Parsons et al., 1994; Saltus and Thompson, 1995; Liu and Stegman, 2012), and development and lengthening of the San Andreas fault transform plate boundary (Atwater and Stock, 1998; DeMets and Merkouriev, 2016). The temporal overlap of these processes with a continental lithosphere primed for extension suggests a causal relationship between these processes and middle Miocene extension across the Basin and Range.

The ignimbrite flareup propagated southward across the northern Basin and Range and northwestward across the southern Basin and Range (e.g., Coney and Reynolds, 1977; Dickinson and Snyder, 1978; Christiansen and Yeats, 1992), reaching the latitudes of the SNNF by middle Miocene time (Fig. 1). In line with the Lund Snee and Miller (2022) hypothesis, we suggest that replacement of the Laramide slab with hot and buoyant asthenosphere at the base of the continental lithosphere and the subsequent heat input from magmatism in the vicinity of the southern Sierra Nevada (i.e., the southern Sierra Nevada, Coso Range, White Mountains, and Mina deflection; Glazner, 2022; Fig. 1) during the middle Miocene weakened the continental lithosphere and resulted in sufficient gravitational potential energy that this part of the Basin and Range was primed for extension. If the southern Sierra Nevada region, as well as the Basin and Range to the east, was primed for extension by the middle Miocene, the western margin of North America must have moved westward to drive that extension.

The plate reconstructions of DeMets and Merkouriev (2016) and Atwater and Stock (1998) and the southwestern North America paleogeographic reconstructions of McQuarrie and Wernicke (2005) and Wernicke and Snow (1998) provide insight into the plate tectonic setting during the middle Miocene and the processes by which the western margin of North America moved west to drive extension. During the middle Miocene, the location of the Mendocino triple junction, relative to the Sierra Nevada–Great Valley block, was at the approximate latitude of the southern part of the Sierra Nevada–Great Valley block (at about the latitude of 36°N today) (Fig. 1). This temporal-spatial constraint indicates that during the middle Miocene, northeast subduction of the Juan de Fuca plate beneath the North America plate characterized the plate boundary west of most of the Sierra Nevada–Great Valley block, and a northwest dextral (transtensional) transform plate boundary between the Pacific and North American plates characterized the plate boundary from the southern extent of the Sierra Nevada–Great Valley block and southward. In this plate configuration, westward motion of the cold and strong Sierra Nevada–Great Valley block, and extension across the Basin and Range to the east and northeast, was probably the result of two plate boundary processes: (1) slab-driven trench retreat along the Juan de Fuca–North America subduction zone boundary (e.g., Humphreys and Coblentz, 2007; Humphreys, 2009; Schellart et al., 2010) and (2) clockwise rotation of the southern ancestral Cascade Range, a consequence of the combination of northwest dextral shear along the lengthening Pacific–North America plate boundary and northeast subduction of the Farallon plate beneath the North American plate (e.g., Magill et al., 1981; Humphreys and Coblentz, 2007; Humphreys, 2009; Wells and McCaffrey, 2013). We suggest that the middle Miocene normal fault slip we have documented along the SNNF, including that documented along the east-adjacent EIFZ (Lee et al., 2009) and WMFZ (Stockli et al., 2003), as well as eastward across the Basin and Range, can be explained by a combination of these lithospheric buoyancy and plate boundary forces.

Preliminary landscape evolution modeling suggesting that the MU transect records a Pliocene episode of normal slip along the SNNF, combined with Pliocene normal fault slip along the east adjacent EIFZ and WMFZ, is consistent with the predicted timing of extension in the premise that upwelling asthenosphere replaced foundering lithosphere mantle beneath the southern Sierra Nevada during the Pliocene (e.g., Ducea and Saleeby, 1996; Liu and Shen, 1998; Manley et al., 2000; Farmer et al., 2002; Saleeby et al., 2003; Jones et al., 2004; Zandt et al., 2004).

The Miocene plate boundary and buoyancy forces we interpret as driving middle Miocene normal fault slip on the SNNF and to the east across the Basin and Range could not have driven the initiation of normal fault slip along the SNNF during late Oligocene and extension in a few localities across the Basin and Range of similar age (Fig. 1H). Prior to the documented late Oligocene extension episodes (Table 3), the ignimbrite flareup had swept southward past all Basin and Range localities, which subsequently recorded late Oligocene extension, except for the SNNF (Figs. 1D and 1H). Following on the Lund Snee and Miller (2022) hypothesis, we suggest that during the late Oligocene between northeast and west-central Nevada, hot and buoyant asthenosphere had replaced the Farallon slab. The subsequent input of heat that drove the ignimbrite flareup thermally weakened the continental lithosphere, increased surface elevation, and increased the gravitational potential energy in this part of the Basin and Range. During the Oligocene, the western margin of the U.S. Cordillera was characterized by oblique subduction of the Farallon plate beneath the North American plate (e.g., Engebretson et al., 1985; Gordon and Jurdy, 1986), and the Pacific plate had just come into contact with the North American plate well south of the Sierra Nevada (Atwater and Stock, 1998). Trench retreat, driven by westward motion of the North American plate (Schellart et al., 2010), along the subduction zone boundary, could have driven the minor late Oligocene-aged extension as the northeast to west-central Nevada part of the Basin and Range was gravitationally unstable, but the southern Sierra Nevada region was not. Why, then, did normal fault slip initiate along the SNNF during the late Oligocene? We speculate that during the late Oligocene, the future SNNF developed along a rheologically weak boundary defined by a late Cretaceous–earliest Paleogene dextral shear zone that had developed within the future Owens Valley region (Bartley et al., 2007)—as well as, perhaps, across the proto–Owens Valley fault which may have recorded an episode of Eocene extension (Sousa, 2019)—and the transition between a low geothermal gradient within the Sierra Nevada to the west (Dumitru, 1990) and higher geothermal gradient to the east. Westward motion of the rigid Sierra Nevada–Great Valley block in the wake of slab rollback resulted in normal fault slip within the late Cretaceous shear zone. Reactivation of the near vertical dextral shear zone by normal fault slip along the SNNF might explain the steep bedrock fault dips observed along SNNF (Fig. 3B). A contributing factor driving this episode of normal faulting may be the buoyancy forces in the Basin and Range to the north and to the south, albeit likely smaller than to the north, which pushed the cold Sierra Nevada–Great Valley block westward with respect to North America (Sonder and Jones, 1999).

CONCLUSIONS

Our integrated structural and new AHe thermochronometric study from the footwall of the SNNF reveals that normal fault slip along the steeply east-dipping SNNF initiated during the late Oligocene and experienced a major second episode of normal slip during the middle Miocene. Preliminary landscape evolution modeling suggests that at least one locality along the SNNF may also record a third episode of normal fault slip during the Pliocene. Evidence for late Oligocene extension across the Basin and Range is limited, suggesting that perhaps this period of extension was relatively minor and local. In contrast, evidence for middle Miocene extension across the Basin and Range is substantial, ranging from the Sierra Nevada on the west to the Wasatch Range on the east, indicating that this period of extension was major and areally extensive. Initiation of normal fault slip along the SNNF during the late Oligocene and continued normal fault slip today indicate that the SNNF is a long-lived western boundary or breakaway zone to the Basin and Range.

Although our AHe studies do not allow us to measure the magnitude of uplift of the Sierra Nevada during the late Cenozoic, since isostasy is likely the major driver of uplift in the footwall of normal faults, the two episodes of normal faulting on the SNNF indicate that the southern Sierra Nevada experienced renewed episodes of uplift during the late Oligocene and middle Miocene, well after the initial episode of uplift in the late Mesozoic–early Cenozoic.

The plate tectonic setting along the western margin of North America and the lithospheric structure in the region of the southern Sierra Nevada changed during the ca. 28–27 Ma slip history on the SNNF. During the late Oligocene, the southern Sierra Nevada was located east of the Farallon–North American subduction zone and well north of the Mendocino Triple Junction. Given this plate configuration, we postulate that trench retreat, driven by westward motion of the North American plate, along the Farallon–North American subduction zone, drove this minor episode of extension across the Basin and Range and the initiation of normal fault slip along the SNNF. During the middle Miocene, the Mendocino Triple Junction had migrated northward so that it was located west of the southern Sierra Nevada (~36° latitude present day), still south of our transects, thus most of Sierra Nevada was located east of the Farallon–North American subduction zone. In this plate configuration, we propose that a combination of northeast subduction of the Farallon plate beneath the North American plate and northwest dextral shear along the Pacific–North American plate boundary resulted in clockwise rotation of North America north of the triple junction. These plate boundary processes, superimposed on a proto–Basin and Range lithosphere primed for extension, drove the middle Miocene slip along the SNNF and extension across the Basin and Range. Since slip along the SNNF was driven by changing plate tectonic settings, the long-term (10^7 yr) average geologic slip rates we estimate for the SNNF cannot be correlated to shorter-term (10^3–10^4 yr) or present-day (10^1 yr) slip rates.

ACKNOWLEDGMENTS

Many thanks to Andrew Yokel-Deluca, Matt Aleksey, and Ben Hodges, who provided invaluable help in the field collecting AHe samples and structural data, and to Andrew Yokel-Deluca, Matt Alekse, Rudra Chatterjee, and Megan Flansburg for their hard work helping process the AHe samples. Discussions with Sam Johnstone on interpreting AHe data were informative. Thanks to Chris Henry for providing the digital shaded relief map base for Figure 1. Craig Jones, Greg Stock, and an anonymous reviewer provided thoughtful and helpful comments that improved this manuscript. Funding was provided by National Science Foundation grants EAR-1753440 (JL), EAR-1753439 (DS), and EAR-1753474 (AB). The stereonet plot was produced using Stereonet 10.2.9 software thanks to Rick Allmendinger.

REFERENCES CITED

Argus, D.F., and Gordon, R.G., 1991, Current Sierra Nevada–North America motion from very long baseline interferometry: Implications for the kinematics of the western United States: Geology, v. 19, no. 11, p. 1085–1088, https://doi.org/10.1130/0091-7613(1991)019<1085:CSNNAM>2.3.CO;2.

Armstrong, P.A., Ehlers, T.A., Chapman, D.S., Farley, K.A., and Kamp, P.J.J., 2003, Exhumation of the central Wasatch Mountains, Utah: 1. Patterns and timing of exhumation deduced from low-temperature thermochronology data: Journal of Geophysical Research, v. 108, p. 2172, https://doi.org/10.1029/2001JB001708.

Armstrong, R.L., and Ward, P., 1991, Evolving geographic patterns of Cenozoic magmatism in the North American Cordillera: The temporal and spatial association of magmatism and metamorphic core complexes: Journal of Geophysical Research, v. 96, p. 13,201–13,224, https://doi.org/10.1029/91JB00412.

Atwater, T., 1970, Implications of plate tectonics for the Cenozoic tectonic evolution of western North America: Geological Society of America Bulletin, v. 81, no. 12, p. 3513–3536, https://doi.org/10.1130/0016-7606(1970)81[3513:IOPTFT]2.0.CO;2.

Atwater, T., and Stock, J., 1998, Pacific–North America plate tectonics of the Neogene southwestern United States: An update: International Geology Review, v. 40, p. 375–402, https://doi.org/10.1080/00206819809465216.

Axelrod, D.I., 1957, Late Tertiary floras and the Sierra Nevadan uplift (California-Nevada): Geological Society of America Bulletin, v. 68, no. 1, p. 19–45, https://doi.org/10.1130/0016-7606(1957)68[19:LTFATS]2.0.CO;2.

Bartley, J.M., Glazner, A.F., Coleman, D.S., Kylander-Clark, A., Mapes, R., and Friedrich, A.M., 2007, Large Laramide dextral offset across Owens Valley, California, and its possible relation to tectonic unroofing of the southern Sierra Nevada, *in* Till, A.B., Roeske, S.M., Sample, J.C., and Foster, D.A., eds., Exhumation Associated with Continental Strike-Slip Fault Systems: Geological Society of America Special Paper 434, p. 129–148, https://doi.org/10.1130/2007.2434(07).

Bateman, P.C., 1965, Geology and tungsten mineralization of the Bishop District California, U.S. Geological Survey Professional Paper 470, 208 p., https://doi.org/10.3133/pp470.

Bateman, P.C., and Wahrhaftig, C., 1966, Geology of the Sierra Nevada, *in* Bailey, E.H., ed., Geology of northern California: California Division of Mines and Geology Bulletin 190, p. 107–172.

Beard, L.S., 1996, Paleogeography of the Horse Spring Formation in relation to the Lake Mead fault system, Virgin Mountains, Nevada and Arizona, *in* Beratan, K.K., ed., Reconstructing the History of Basin and Range Extension Using Sedimentology and Stratigraphy: Geological Society of America Special Paper 303, p. 27–60, https://doi.org/10.1130/0-8137-2303-5.27.

Belton, D.X., Kohn, B.P., and Gleadow, A.J.W., 2004, Quantifying "excess helium": Some of the issues and assumptions in combined (U-Th)/He and fission track analysis, *in* Andressien, P., ed.: Amsterdam, Tenth International Fission Track Dating Conference, p. 18, abstract code DVL-12-O.

Beltrando, M., Stockli, D.F., Decarlis, A., and Mantschal, G., 2015, A crustal-scale view at rift localization along the fossil Adriatic margin of the Alpine Tethys preserved in NW Italy: Tectonics, v. 34, p. 1927–1951, https://doi.org/10.1002/2015TC003973.

Bennett, R.A., Wernicke, B.P., Niemi, N.A., Friedrich, A.M., and Davis, J.L., 2003, Contemporary strain rates in the northern Basin and Range province from GPS data: Tectonics, v. 22, no. 2, 31 p., https://doi.org/10.1029/2001TC001355.

Berry, M.E., 1997, Geomorphic analysis of late Quaternary faulting on Hilton Creek, Round Valley, and Coyote warp faults, east-central Sierra Nevada, California, USA: Geomorphology, v. 20, p. 177–195, https://doi.org/10.1016/S0169-555X(97)00033-0.

Best, M.G., and Christiansen, E.H., 1991, Limited extension during peak Tertiary volcanism, Great Basin of Nevada and Utah: Journal of Geophysical Research, v. 96, p. 13,509–13,528, https://doi.org/10.1029/91JB00244.

Best, M.G., and Hamblin, W.K., 1978, Origin of the northern Basin and Range Province: Implications from the geology of its eastern boundary, *in* Smith, R.B., and Eaton, G.P., Cenozoic Tectonics and Regional Geophysics of the Western Cordillera: Geological Society of America Memoir 152, p. 313–340, https://doi.org/10.1130/MEM152-p313.

Bidgoli, T.S., Amir, E., Walker, J.D., Stockli, D.F., Andrew, J.E., and Caskey, S.J., 2015, Low-temperature thermochronology of the Black and Panamint mountains, Death Valley, California: Implications for geodynamic controls on Cenozoic intraplate strain: Lithosphere, v. 7, p. 473–480, https://doi.org/10.1130/L406.1.

Buck, W.R., 1988, Flexural rotation of normal faults: Tectonics, v. 7, p. 959–973, https://doi.org/10.1029/TC007i005p00959.

Busby, C.J., Hagan, J.C., and Renne, P., 2013, Initiation of Sierra Nevada range front–Walker Lane faulting ca. 12 Ma in the Ancestral Cascades arc: Geosphere, v. 9, no. 5, p. 1125–1146, https://doi.org/10.1130/GES00927.1.

Camp, V.E., Pierce, K.L., and Morgan, L.A., 2015, Yellowstone plume trigger for Basin and Range extension, and coeval emplacement of the Nevada–Columbia Basin magmatic belt: Geosphere, v. 11, no. 2, p. 203–225, https://doi.org/10.1130/GES01051.1.

Cashman, P.H., Trexler, J.H., Jr., Muntean, T.W., Faulds, J.E., Louie, J.N., and Oppliger, G.L., 2009, Neogene tectonic evolution of the Sierra Nevada–Basin and Range transition zone at the latitude of Carson City, Nevada, *in* Oldow, J.S., and Cashman, P.H., eds., Late Cenozoic Structure and Evolution of the Great Basin–Sierra Nevada Transition: Geological Society of America Special Paper 447, p. 171–188, https://doi.org/10.1130/2009.2447(10).

Cassel, E.J., and Graham, S.A., 2011, Paleovalley morphology and fluvial system evolution of Eocene–Oligocene sediments ("auriferous gravels"), northern Sierra Nevada, California: Implications for climate, tectonics, and topography: Geological Society of America Bulletin, v. 123, no. 9–10, p. 1699–1719, https://doi.org/10.1130/B30356.1.

Cassel, E.J., Graham, S.A., and Chamberlain, C.P., 2009, Cenozoic tectonic and topographic evolution of the northern Sierra Nevada, California, through stable isotope paleoaltimetry in volcanic glass: Geology, v. 37, no. 6, p. 547–550, https://doi.org/10.1130/G25572A.1.

Cassel, E.J., Grove, J., and Graham, S.A., 2012a, Eocene drainage evolution and erosion of the Sierra Nevada batholith across northern California and Nevada: American Journal of Science, v. 312, p. 117–144, https://doi.org/10.2475/02.2012.03.

Cassel, E.J., Graham, S.A., Chamberlain, C.P., and Henry, C.D., 2012b, Early Cenozoic topography, morphology, and tectonics of the northern Sierra Nevada and western Basin and Range: Geosphere, v. 8, no. 2, p. 229–249, https://doi.org/10.1130/GES00671.1.

Cecil, M.R., Ducea, M.N., Reiners, P.W., and Chase, C.G., 2006, Cenozoic exhumation of the northern Sierra Nevada, California, from (U-Th)/He thermochronology: Geological Society of America Bulletin, v. 118, no. 11–12, p. 1481–1488, https://doi.org/10.1130/B25876.1.

Chase, C.G., and Wallace, T.C., 1986, Uplift of the Sierra Nevada of California: Geology, v. 14, p. 730–733, https://doi.org/10.1130/0091-7613(1986)14<730:UOTSNO>2.0.CO;2.

Chen, J.H., and Moore, J.G., 1982, Uranium-lead isotopic ages from the Sierra Nevada batholith: Journal of Geophysical Research, v. 87, p. 4761–4784, https://doi.org/10.1029/JB087iB06p04761.

Christensen, M.N., 1966, Late Cenozoic crustal movements in the Sierra Nevada of California: Geological Society of America Bulletin, v. 77, no. 2, p. 163–182, https://doi.org/10.1130/0016-7606(1966)77[163:LCCMIT]2.0.CO;2.

Christiansen, R.L., and Yeats, R.S., 1992, Post-Laramide geology of the U.S. Cordilleran region, *in* Burchfiel, B.C., Lipman, P.W., and Zoback, M.L., eds., The Cordilleran orogen—Conterminous U.S.: Boulder, Colorado, Geological Society of America, Geology of North America, v. G-3, p. 261–406, https://doi.org/10.1130/DNAG-GNA-G3.261.

Clark, M.K., Mahéo, G., Saleeby, J., and Farley, K.A., 2005, The non-equilibrium landscape of the southern Sierra Nevada, California: GSA Today, v. 15, no. 9, p. 4–10, https://doi.org/10.1130/1052-5173(2005)015<4:TNELOT>2.0.CO;2.

Colgan, J.P., and Henry, C.D., 2009, Rapid middle Miocene collapse of the Mesozoic orogenic plateau in north-central Nevada: International Geology Review, v. 51, p. 920–961, https://doi.org/10.1080/00206810903056731.

Colgan, J.P., Dumitru, T.A., McWilliams, M., and Miller, E.L., 2006, Timing of Cenozoic volcanism and Basin and Range extension in northwestern Nevada: New constraints from the northern Pine Forest Range: Geology, v. 118, no. 1–2, p. 126–139, https://doi.org/10.1130/B25681.1.

Colgan, J.P., John, D.A., Henry, C.D., and Fleck, R.J., 2008, Large-magnitude Miocene extension of the Eocene Caetano caldera, Shoshone and Toiyabe Ranges, Nevada: Geosphere, v. 4, no. 1, p. 107–130, https://doi.org/10.1130/GES00115.1.

Colgan, J.P., Howard, K.A., Fleck, R.J., and Wooden, J.L., 2010, Rapid middle Miocene extension and unroofing of the southern Ruby Mountains, Nevada: Tectonics, v. 29, TC6022, https://doi.org/10.1029/2009TC002655.

Colgan, J.P., Johnstone, S.A., and Shuster, D.L., 2020, Timing of Cenozoic extension in the southern Stillwater Range and Dixie Valley, Nevada: Tectonics, v. 39, no. 3, 18 p., https://doi.org/10.1029/2019TC005757.

Coney, P.J., and Harms, T.A., 1984, Cordilleran metamorphic core complexes: Cenozoic extensional relics of Mesozoic compression: Geology, v. 12, no. 9, p. 550–554, https://doi.org/10.1130/0091-7613(1984)12<550:CMCCCE>2.0.CO;2.

Coney, P.J., and Reynolds, S.J., 1977, Cordilleran Benioff zones: Nature, v. 270, p. 403–406, https://doi.org/10.1038/270403a0.

Crough, S.T., and Thompson, G.A., 1977, Upper mantle origin of Sierra Nevada uplift: Geology, v. 5, no. 7, p. 396–399, https://doi.org/10.1130/0091-7613(1977)5<396:UMOOSN>2.0.CO;2.

DeCelles, P.G., 2004, Late Jurassic to Eocene evolution of the Cordilleran thrust belt and foreland basin system, western USA: American Journal of Science, v. 304, p. 105–168, https://doi.org/10.2475/ajs.304.2.105.

DeMets, C., and Merkouriev, S., 2016, High-resolution reconstructions of Pacific–North American plate motion: 20 Ma to present: Geophysical Journal International, v. 207, p. 741–773, https://doi.org/10.1093/gji/ggw305.

Dickinson, W.R., 1997, Overview: Tectonic implications of Cenozoic volcanism in coastal California: Geological Society of America Bulletin, v. 109, no. 8, p. 936–954, https://doi.org/10.1130/0016-7606(1997)109<0936:OTIOCV>2.3.CO;2.

Dickinson, W.R., 2002, The Basin and Range province as a composite extensional domain: International Geology Review, v. 44, p. 1–38, https://doi.org/10.2747/0020-6814.44.1.1.

Dickinson, W.R., and Snyder, W.S., 1978, Plate tectonics of the Laramide orogeny, *in* Matthews, V., III, ed., Laramide Folding Associated with Basement Block Faulting in the Western United States: Geological Society of America Memoir 151, p. 355–366, https://doi.org/10.1130/MEM151-p355.

Dickinson, W.R., and Snyder, W.S., 1979, Geometry of subducted slabs related to San Andreas transform: The Journal of Geology, v. 87, p. 609–627, https://doi.org/10.1086/628456.

Dilles, J.H., and Gans, P.B., 1995, The chronology of Cenozoic volcanism and deformation in the Yerington area, western Basin and Range and Walker Lane: Geological Society of America Bulletin, v. 107, no. 4, p. 474–486, https://doi.org/10.1130/0016-7606(1995)107<0474:TCOCVA>2.3.CO;2.

Dixon, T.H., Miller, M., Farina, F., Wang, H., and Johnson, D., 2000, Present-day motion of the Sierra Nevada block and some tectonic implications for the Basin and Range province, North American Cordillera: Tectonics, v. 19, p. 1–24, https://doi.org/10.1029/1998TC001088.

Du Bray, E.A., and Moore, J.G., 1985, Geologic map of the Olancha Quadrangle, southern Sierra Nevada, California: U.S. Geological Survey Miscellaneous Field Studies, Map MF-1734, scale 1:62,500, https://doi.org/10.3133/mf1734.

Du Bray, E.A., John, D.A., and Cousens, B.L., 2014, Petrologic, tectonic, and metallogenic evolution of the southern segment of the ancestral Cascades magmatic arc, California and Nevada: Geosphere, v. 10, no. 1, p. 1–39, https://doi.org/10.1130/GES00944.1.

Ducea, M.N., and Saleeby, J.B., 1996, Buoyancy sources for a large, unrooted mountain range, the Sierra Nevada, California: Evidence from xenoliths thermobarometry: Journal of Geophysical Research, v. 101, p. 8229–8244, https://doi.org/10.1029/95JB03452.

Ducea, M.N., and Saleeby, J.B., 1998a, The age and origin of a thick mafic-ultramafic keel from beneath the Sierra Nevada batholith: Contributions to Mineralogy and Petrology, v. 133, p. 169–185, https://doi.org/10.1007/s004100050445.

Ducea, M., and Saleeby, J., 1998b, A case for delamination of the deep batholithic crust beneath the Sierra Nevada: International Geology Review, v. 40, p. 78–93, https://doi.org/10.1080/00206819809465199.

Dumitru, T.A., 1990, Subnormal Cenozoic geothermal gradients in the extinct Sierra Nevada magmatic arc: Consequences of Laramide and post-Laramide shallow-angle subduction: Journal of Geophysical Research, v. 95, p. 4925–4941, https://doi.org/10.1029/JB095iB04p04925.

Egan, S.S., 1992, The flexural isostatic response of the lithosphere to extension tectonics: Tectonophysics, v. 202, p. 291–308, https://doi.org/10.1016/0040-1951(92)90115-M.

Ehlers, T.A., Willett, S.D., Armstrong, P.A., and Chapman, D.S., 2003, Exhumation of the central Wasatch Mountains, Utah: 2. Thermokinematic model of exhumation, erosion, and thermochronometer interpretation: Journal of Geophysical Research, v. 108, p. 2173, https://doi.org/10.1029/2001JB001723.

Engebretson, D.C., Cox, A., and Gordon, R.G., 1985, Relative Motions between Oceanic and Continental Plates in the Pacific Basin: Geological Society America Special Paper 206, 59 p., https://doi.org/10.1130/SPE206-p1.

Evans, S.L., Styron, R.H., van Soest, J.C., Hodges, K.V., and Hanson, A.D., 2015, Zircon and apatite (U-Th)/He evidence for Paleogene and Neogene extension in the southern Snake Range, Nevada, USA: Tectonics, v. 34, p. 2142–2164, https://doi.org/10.1002/2015TC003913.

Farley, K.A., 2000, Helium diffusion from apatite: General behavior as illustrated by Durango fluorapatite: Journal of Geophysical Research, v. 105, p. 2903–2914, https://doi.org/10.1029/1999JB900348.

Farmer, G.L., Glazner, A.F., and Manley, C.R., 2002, Did lithospheric delamination trigger late Cenozoic potassic volcanism in the southern Sierra Nevada, California?: Geological Society of America Bulletin, v. 114, no. 6, p. 754–768, https://doi.org/10.1130/0016-7606(2002)114<0754:DLDTLC>2.0.CO;2.

Faulds, J.E., Feuerback, D.L., Reagan, M.K., Metcalf, R.V., Gans, P., and Walker, J.D., 1995, The Mount Perkins block, northwestern Arizona: An exposed cross-section of an evolving, pre-extensional to synextensional magmatic system: Journal of Geophysical Research, v. 100, p. 15,249–15,266, https://doi.org/10.1029/95JB01375.

Faulds, J.E., Olson, E.L., Harlan, S.S., and McIntosh, W.C., 2002, Miocene extension and fault-related folding in the Highland Range, southern Nevada: A three-dimensional perspective: Journal of Structural Geology, v. 24, p. 861–886, https://doi.org/10.1016/S0191-8141(01)00116-X.

Faulds, J.E., Price, L.M., Snee, L.W., and Gans, P.B., 2010, A chronicle of Miocene extension near the Colorado Plateau-Basin and Range boundary, southern White Hills, northwestern Arizona: Paleogeographic and tectonic implications, *in* Umhoefer, P.J., Beard, L.S., and Lamb, M.A., eds., Miocene Tectonics of the Lake Mead Region, Central Basin and Range: Geological Society of America Special Paper 463, p. 87–119, https://doi.org/10.1130/2010.2463(05).

Fitzgerald, P.G., 1992, The Transantarctic Mountains of southern Victoria Land: The application of apatite fission track analysis to a rift shoulder uplift: Tectonics, v. 11, p. 634–662, https://doi.org/10.1029/91TC02495.

Fitzgerald, P.G., Fryxell, J.E., and Wernicke, B.P., 1991, Miocene crustal extension and uplift in southeastern Nevada: Constraints from fission track analysis: Geology, v. 19, no. 10, p. 1013–1016, https://doi.org/10.1130/0091-7613(1991)019<1013:MCEAUI>2.3.CO;2.

Flowers, R.M., Ketcham, R.A., Shuster, D.L., and Farley, K.A., 2009, Apatite (U-Th)/He thermochronometry using a radiation damage accumulation and annealing model: Geochimica et Cosmochimica Acta, v. 73, p. 2347–2365, https://doi.org/10.1016/j.gca.2009.01.015.

Fosdick, J.C., and Colgan, J.P., 2008, Miocene extension in the East Range, Nevada: A two-stage history of normal faulting in the northern Basin and Range: Geological Society of America Bulletin, v. 120, no. 9–10, p. 1198–1213, https://doi.org/10.1130/B26201.1.

Foster, D.A. and Gleadow, A.J.W., 1996, Structural framework and denudation history of the flanks of the Kenya and Anza Rifts, east Africa: Tectonics, v. 15, p. 258–271, https://doi.org/10.1029/95TC02744.

Gans, P.B., Mahood, G.A., and Schermer, E., 1989, Synextensional Magmatism in the Basin and Range Province: A Case Study from the Eastern Great Basin: Geological Society of America Special Paper 233, 53 p., https://doi.org/10.1130/SPE233-p1.

Garside, L.J., Henry, C.D., Faulds, J.E., and Hinz, N.H., 2005, The upper reaches of the Sierra Nevada auriferous gold channels, California and Nevada: Geological Society of Nevada Symposium, p. 209–235.

Glazner, A.F., 2022, Cenozoic magmatism and plate tectonics in western North America: Have we got it wrong?, *in* Foulger, G.R., Hamilton, L.C., Jurdy, D.M., Stein, C.A., Howard, K.A., and Stein, S., eds., In the Footsteps of Warren B. Hamilton: New Ideas in Earth Science: Geological Society of America Special Paper 553, p. 95–108, https://doi.org/10.1130/2021.2553(09).

Gonsior, Z.J., and Dilles, J.H., 2008, Timing and evolution of Cenozoic extensional normal faulting and magmatism in the southern Tobin Range, Nevada: Geosphere, v. 4, no. 4, p. 687–712, https://doi.org/10.1130/GES00137.1.

Gordon, R.G., and Jurdy, D.M., 1986, Cenozoic global plate motions: Journal of Geophysical Research, v. 91, p. 12,389–12,406, https://doi.org/10.1029/JB091iB12p12389.

Gorynski, K.E., Stockli, D.F., and Walker, J.D., 2013, Thermochronometrically constrained anatomy and evolution of a Miocene extensional accommodation zone and tilt domain boundary: The southern Wassuk Range, Nevada: Tectonics, v. 32, p. 516–539, https://doi.org/10.1002/tect.20044.

Gorynski, K.E., Walker, J.D., Stockli, D.F., and Sabin, A., 2014, Apatite (U–Th)/He thermochronometry as an innovative geothermal exploration tool: A case study from the southern Wassuk Range, Nevada: Journal of Volcanology and Geothermal Research, v. 270, p. 99–114, https://doi.org/10.1016/j.jvolgeores.2013.11.018.

Hammond, W.C., Blewitt, G., and Kreemer, C., 2016, GPS Imaging of vertical land motion in California and Nevada: Implications for Sierra Nevada uplift: Journal of Geophysical Research: Solid Earth, v. 121, p. 7681–7703, https://doi.org/10.1002/2016JB013458.

Henry, C.D., 2008, Ash-flow tuffs and paleovalleys in northeastern Nevada: Implications for Eocene paleogeography and extension in the Sevier hinterland, northern Great Basin: Geosphere, v. 4, no. 1, p. 1–35, https://doi.org/10.1130/GES00122.1.

Henry, C.D., and Faulds, J.E., 2010, Ash-flow tuffs in the Nine Hill, Nevada, paleovalley and implications for tectonism and volcanism of the western Great Basin, USA: Geosphere, v. 6, no. 4, p. 339–369, https://doi.org/10.1130/GES00548.1.

Henry, C.D., and John, D.A., 2013, Magmatism, ash-flow tuffs, and calderas of the ignimbrite flareup in the western Nevada volcanic field, Great Basin, USA: Geosphere, v. 9, no. 4, p. 951, https://doi.org/10.1130/GES00867.1.

Henry, C.D. and Perkins, M.E., 2001, Sierra Nevada–Basin and Range transition near Reno, Nevada: Two-stage development at 12 and 3 Ma: Geology, v. 29, no. 8, p. 719–722, https://doi.org/10.1130/0091-7613(2001)029<0719:SNBART>2.0.CO;2.

Henry, C.D., Hinz, N.H., Faulds, J.E., Colgan, J.P., John, D.A., Brooks, E.R., Cassel, E.J., Garside, L.J., Davis, D.A., and Castor, S.B., 2012, Eocene–Early Miocene paleotopography of the Sierra Nevada–Great Basin–Nevadaplano based on widespread cash-flow tuffs and paleovalleys: Geosphere, v. 8, no. 1, p. 1–27, https://doi.org/10.1130/GES00727.1.

Hildreth, W., Fierstein, J., Phillips, F.M., and Calvert, A., 2022, Trachyandesite of Kennedy Table, its vent complex, and post–9.3 Ma uplift of the central Sierra Nevada: Geological Society of America Bulletin, v. 134, no. 5–6, p. 1143–1159, https://doi.org/10.1130/B36125.1.

House, M.A., Wernicke, B.P., Farley, K.A., and Dumitru, T.A., 1997, Cenozoic thermal evolution of the central Sierra Nevada, from (U-Th)/He thermochronometry: Earth and Planetary Science Letters, v. 151, p. 167–179, https://doi.org/10.1016/S0012-821X(97)81846-8.

House, M.A., Wernicke, B.P., and Farley, K.A., 1998, Dating topography of the Sierra Nevada, California, using apatite (U-Th)/He ages: Nature, v. 396, p. 66–69, https://doi.org/10.1038/23926.

House, M.A., Wernicke, B.P., and Farley, K.A., 2001, Paleo-geomorphology of the Sierra Nevada, California, from the (U-Th)/He ages in apatite: American Journal of Science, v. 301, p. 77–102, https://doi.org/10.2475/ajs.301.2.77.

Huber, N.K., 1981, Amount and timing of late Cenozoic uplift and tilt of the central Sierra Nevada, California—Evidence from the upper San Joaquin River basin: U.S. Geological Survey Professional Paper 1197, 28 p., https://doi.org/10.3133/pp1197.

Humphreys, E.D., 1995, Post-Laramide removal of the Farallon slab, western United States: Geology, v. 23, no. 11, p. 987–990, https://doi.org/10.1130/009–7613(1995)023<0987:PLROTF>2.3.CO;2.

Humphreys, E.D., 2009, Relation of flat slab subduction to magmatism and deformation in the western United States, *in* Kay, S.M., Ramos, V.A., and Dickinson, W.R., eds., Backbone of the Americas: Shallow Subduction, Plateau Uplift, and Ridge and Terrane Collision: Geological Society of America Memoir 204, p. 85–98, https://doi.org/10.1130/2009.1204(04).

Humphreys, E.D., and Coblentz, D.D., 2007, North American dynamics and western U.S. tectonics: Reviews of Geophysics, v. 45, RG3001, https://doi.org/10.1029/2005RG000181.

John, D.A., Thomason, R.E., and McKee, E.H., 1989, Geology and K-Ar geochronology of the Paradise Peak Mine and the relationship of pre–Basin and Range extension to early Miocene precious metal mineralization in west-central Nevada: Economic Geology, v. 84, p. 631–649, https://doi.org/10.2113/gsecongeo.84.3.631.

John, D.A., Du Bray, E.A., Blakely, R.J., Fleck, R.J., Vikre, P.G., Box, S.E., and Moring, B.C., 2012, Miocene magmatism in the Bodie Hills volcanic field, California and Nevada: A long-lived eruptive center in the southern segment of the ancestral Cascades arc: Geosphere, v. 8, no. 1, p. 44–97, https://doi.org/10.1130/GES00674.1.

Johnstone, S.A., and Colgan, J.P., 2018, Interpretation of low-temperature thermochronometer ages from tilted normal fault blocks: Tectonics, v. 37, p. 3647–3667, https://doi.org/10.1029/2018TC005207.

Jones, C.H., Sonder, L.J., and Unruh, J.R., 1998, Lithospheric gravitational potential energy and past orogenesis: Implications for conditions of initial basin and range and Laramide deformation: Geology, v. 26, no. 7, p. 639–642, https://doi.org/10.1130/0091-7613(1998)026<0639:LGPEAP>2.3.CO;2.

Jones, C.H., Farmer, G.L., and Unruh, J.R., 2004, Tectonics of Pliocene removal of lithosphere of the Sierra Nevada, California: Geological Society of America Bulletin, v. 116, no. 11–12, p. 1408–1422, https://doi.org/10.1130/B25397.1.

Kamola, D.L., Walker, J.D., Monastero, F.C., and Stockli, D.F., 2005, Evidence from Indian Wells Valley and Coso Range for Miocene initiation of the eastern escarpment of the southern Sierra Nevada, California: Geological Society of America Abstracts with Programs, v. 37, p. 203.

King, G., and Ellis, M., 1990, The origin of large local uplift in extensional regions: Nature, v. 348, p. 689–693, https://doi.org/10.1038/348689a0.

Koerner, A., Busby, C., Putirka, K., and Pluhar, C.J., 2009, New evidence for alternating effusive and explosive eruptions from the type section of the Stanislaus Group in the 'Cataract' palaeocanyon, central Sierra Nevada: International Geology Review, v. 51, p. 962–985, https://doi.org/10.1080/00206810903028185.

Konstantinou, A., Strickland, A., Miller, E.L., and Wooden, J.W., 2012, Multi-stage Cenozoic extension of the Albion–Raft River–Grouse Creek metamorphic core complex: Geochronologic and stratigraphic constraints: Geosphere, v. 8, no. 6, p. 1429–1466, https://doi.org/10.1130/GES00778.1.

Le, K., Lee, J., Owen, L., and Finkel, R.C., 2007, Late Quaternary slip rates along the Sierra Nevada frontal fault zone, California: Evidence for slip partitioning across the western margin of the Eastern California Shear Zone–Basin and Range Province: Geological Society of America Bulletin, v. 119, no. 1–2, p. 240–256, https://doi.org/10.1130/B25960.1.

LeConte, J., 1886, A post-Tertiary elevation of the Sierra Nevada shown by the river beds: American Journal of Science, v. 32, p. 167–181, https://doi.org/10.2475/ajs.s3-32.189.167.

Lee, J., Stockli, D.F., Owen, L.A., Finkel, R.C., and Kislitsyn, R., 2009, Exhumation of the Inyo Mountains, California: Implications for the timing of extension along the western boundary of the Basin and Range Province and distribution of dextral fault slip rates across the eastern California shear zone: Tectonics, v. 28, TC1001, https://doi.org/10.1029/2008TC002295.

Lee, J., Hoxey, A.H., Calvert, A., and Dubyoski, P., 2020, Plate boundary trench retreat and dextral shear drive intracontinental fault slip histories: Neogene dextral faulting across the Gabbs Valley and Gillis Ranges, Central Walker Lane, Nevada, Geosphere, v. 16, no. 5, https://doi.org/10.1130/GES02240.1.

Lee, J., Stockli, D., Blythe, A., and Fox, M., 2021, Cenozoic slip along the southern Sierra Nevada range front normal fault, California: A long-lived stable western boundary of the Basin and Range: Geological Society of America Abstracts with Programs, v. 53, https://doi.org/10.1130/abs/2021CD-363159.

Lindgren, W., 1911, The Tertiary gravels of the Sierra Nevada of California: U.S. Geological Survey Professional Paper 73, 226 p., https://doi.org/10.3133/pp73.

Lippolt, H.J., Leitz, M., Wernicke, R.S., and Hagedorn, B., 1994, (Uranium + thorium)/helium dating of apatite: Experience with samples from different geochemical environments: Chemical Geology: Isotope Geoscience, v. 112, no. 1–2, p. 179–191, https://doi.org/10.1016/0009-2541(94)90113-9.

Liu, L., and Stegman, D.R., 2012, Origin of Columbia River flood basalt controlled by propagating rupture of the Farallon slab: Nature, v. 482, p. 386–389, https://doi.org/10.1038/nature10749.

Liu, M., and Shen, Y., 1998, Sierra Nevada uplift: A ductile link to mantle upwelling under the Basin and Range province: Geology, v. 26, no. 4, p. 299–302, https://doi.org/10.1130/0091-7613(1998)026<0299:SNUADL>2.3.CO;2.

Loomis, D.P., and Burbank, D.W., 1988, The stratigraphic evolution of the El Paso basin, southern California: Implications for the Miocene development of the Garlock fault and uplift of the Sierra Nevada: Geological Society of America Bulletin, v. 100, no. 1, p. 12–28, https://doi.org/10.1130/0016-7606(1988)100<0012:TSEOTE>2.3.CO;2.

Long, S.P., and Walker, J.P., 2015, Geometry and kinematics of the Grant Range brittle detachment system, eastern Nevada, U.S.A.: An endmember style of upper-crustal extension: Tectonics, v. 34, p. 1837–1862, https://doi.org/10.1002/2015TC003918.

Long, S.P., Heizler, M.T., Thomson, S.N., Reiners, P.W., and Fryxell, J.E., 2018, Rapid Oligocene to Early Miocene extension along the Grant Range detachment system, Nevada, USA: Insights from multipart cooling histories of footwall rocks: Tectonics, v. 37, p. 4752–4779, https://doi.org/10.1029/2018TC005073.

Lund Snee, J.-E., and Miller, E.L., 2022, Magmatism, migrating topography, and the transition from Sevier shortening to Basin and Range extension, western United States, *in* Craddock, J.P., Malone, D.H., Foreman, B.Z., and Konstantinou, A., eds., Tectonic Evolution of the Sevier-Laramide Hinterland, Thrust Belt, and Foreland, and Postorogenic Slab Rollback (180–20 Ma): Geological Society of America Special Paper 555, https://doi.org/10.1130/2021.2555(13).

Lund Snee, J.-E., Miller, E.L., Grove, M., Hourigan, J.K., and Konstantinou, A., 2016, Cenozoic paleogeographic evolution of the Elko Basin and surrounding region, northeast Nevada: Geosphere, v. 12, no. 2, p. 464–500, https://doi.org/10.1130/GES01198.1.

Magill, J., Cox, A., and Duncan, R., 1981, Tillamook volcanic series: Further evidence for tectonic rotation of the Oregon Coast Range: Journal of Geophysical Research, v. 86, p. 2953–2970, https://doi.org/10.1029/JB086iB04p02953.

MacGinitie, H.D., 1941, A Middle Eocene Flora from the Central Sierra Nevada: Carnegie Institute of Washington Publication 534, 178 p.

MacNamee, A.F., 2015, Thermochronometric investigation of structural evolution and geothermal systems in extensional settings, Dixie Valley, Nevada [M.S. thesis]: Austin, Texas, University of Texas, 166 p.

Manley, C.R., Glazner, A.F., and Farmer, G.L., 2000, Timing of volcanism in the Sierra Nevada of California: Evidence for Pliocene delamination of the batholithic root?: Geology, v. 28, no. 9, p. 811–814, https://doi.org/10.1130/0091-7613(2000)28<811:TOVITS>2.0.CO;2.

Martel, S.J., Stock, G.M., and Ito, G., 2014, Mechanics of relative and absolute displacements across normal faults, and implications for uplift and subsidence along the eastern escarpment of the Sierra Nevada, California: Geosphere, v. 10, no. 2, p. 243–263, https://doi.org/10.1130/GES00968.1.

McCosby, J.B., 2019, Characterizing the deformation history of the southern Mina Deflection: Field and structural studies in the Huntoon Mountains, California-Nevada [M.S. thesis]: Ellensburg, Washington, Central Washington University, 65 p.
McGrew, A., and Metcalf, J., 2021, Episodic late Eocene to Recent extension in the vicinity of the Ruby Mountains and East Humbolt Range, Elko County, Nevada: Geological Society of America Abstracts with Programs, v. 53, https://doi.org/10.1130/abs/2021CD-363293.
McPhillips, D., and Brandon, M.T., 2012, Topographic evolution of the Sierra Nevada measured directly by inversion of low-temperature thermochronology: American Journal of Science, v. 312, p. 90–116, https://doi.org/10.2475/02.2012.02.
McQuarrie, N., and Wernicke, B.P., 2005, An animated tectonic reconstruction of southwestern North America since 36 Ma: Geosphere, v. 1, no. 3, p. 147–172, https://doi.org/10.1130/GES00016.1.
Miller, E.L., Dumitru, T.A., Brown, R.W., and Gans, P.B., 1999, Rapid Miocene slip on the Snake Range-Deep Creek range fault system, east-central Nevada: Geological Society of America Bulletin, v. 111, no. 6, p. 886–905, https://doi.org/10.1130/0016–7606(1999)111<0886: RMSOTS>2 .3.CO;2.
Montgomery, D.R., 1994, Valley incision and the uplift of mountain peaks: Journal of Geophysical Research, v. 99, p. 13,913–13,921, https://doi.org/10.1029/94JB00122.
Moore, J.G., 1981, Geologic map of the Mount Whitney quadrangle, Inyo and Tulare counties, California: U.S. Geological Survey GQ-1545, scale 1:62,500, https://doi.org/10.3133/gq1545.
Mulch, A., Graham, S.A., and Chamberlain, C.P., 2006, Hydrogen Isotopes in Eocene River Gravels and Paleoelevation of the Sierra Nevada: Science, v. 313, no. 5738, p. 87–89, https://doi.org/10.1126/science.1125986.
Oldow, J.S., Elias, E.A., Ferranti, L., McClelland, W.C., and McIntosh, W.C., 2009, Late Miocene to Pliocene synextensional deposition in fault-bounded basins within the upper plate of the western Silver Peak–Lone Mountain extensional complex, west-central Nevada, *in* Oldow, J.S., and Cashman, P.H., eds., Late Cenozoic Structure and Evolution of the Great Basin–Sierra Nevada Transition: Geological Society of America Special Paper 447, p. 275–312, https://doi.org/10.1130/2009.2447(14).
Page, B.M., Thompson, G.A., and Coleman, R.G., 1998, Late Cenozoic tectonics of the central and southern Coast Ranges of California: Geological Society of America Bulletin, v. 110, no. 7, p. 846–876, https://doi.org/10.1130/0016-7606(1998)110<0846:OLCTOT>2.3.CO;2.
Parsons, T., Thompson, G.A., and Sleep, N.H., 1994, Mantle plume influence on the Neogene uplift and extension of the U.S. western Cordillera?: Geology, v. 22, no. 1, p. 83–86, https://doi.org/10.1130/0091-7613(1994)022<0083:MPIOTN>2.3.CO;2.
Pelletier, J.D., 2007, Numerical modeling of the Cenozoic geomorphic evolution of the southern Sierra Nevada, California: Earth and Planetary Science Letters, v. 259, no. 1–2, p. 85–96, https://doi.org/10.1016/j.epsl.2007.04.030.
Phillips, F.M., and Majkowski, L., 2011, The role of low-angle normal faulting in active tectonics of the northern Owens Valley, California: Lithosphere, v. 3, no. 1, p. 22–36, https://doi.org/10.1130/L73.1.
Pluhar, C.J., Deino, A.L., King, N.M., Busby, C., Hausback, B.P., Wright, T., and Fischer, C., 2009, Lithostratigraphy, magnetostratigraphy, and radiometric dating of the Stanislaus Group, CA, and age of the Little Walker Caldera: International Geology Review, v. 51, p. 873–899, https://doi.org/10.1080/00206810902945017.
Poage, M.A., and Chamberlain, C.P., 2002, Stable isotopic evidence for a pre-middle Miocene rain shadow in the western Basin and Range: Implication for the paleotopography of the Sierra Nevada: Tectonics, v. 21, no. 4, https://doi.org/10.1029/2001TC001303.
Proffett, J.M., Jr., 1977, Cenozoic geology of the Yerington district, Nevada, and implications for the nature and origin of Basin and Range faulting: Geological Society of America Bulletin, v. 88, no. 2, p. 247–266, https://doi.org/10.1130/0016-7606(1977)88<247:CGOTYD>2.0.CO;2.
Reiners, P.W., Brady, R., Farley, K.A., Fryxell, J.E., Wernicke, B., and Lux, D., 2000, Helium and argon thermochronometry of the Gold Butte block, South Virgin Mountains, Nevada: Earth and Planetary Science Letters, v. 178, p. 315–326, https://doi.org/10.1016/S0012-821X(00)00080-7.
Ruppert, R.F., Faulds, J.E., Miller, C.F., and Heizler, M., 1999, Interplay between magmatism and N-S and E-W extension, northern Newberry Mountains, southern Nevada: Geological Society of America Abstracts with Programs, v. 30, p. 90.
Saleeby, J., Ducea, M., and Clemens-Knott, D., 2003, Production and loss of high-density batholithic root, southern Sierra Nevada, California: Tectonics, v. 22, no. 6, 24 p., https://doi.org/10.1029/2002TC001374.
Saleeby, J., Le Pourhiet, L., Saleeby, Z., and Gurnis, M., 2012, Epeirogenic transients related to mantle lithosphere removal in the southern Sierra Nevada region, California: Part I. Implications of thermomechanical modeling: Geosphere, v. 8, no. 6, p. 1286–1309, https://doi.org/10.1130/GES00746.1.
Saleeby, J., Saleeby, Z., and Le Pourhiet, L., 2013, Epeirogenic transients related to mantle lithosphere removal in the southern Sierra Nevada region, California: Part II. Implications of rock uplift and basin subsidence relations: Geosphere, v. 9, no. 3, p. 394–425, https://doi.org/10.1130/GES00816.1.
Saleeby, J.B., 1981, Ocean floor accretion and volcanoplutonic arc evolution of the Mesozoic Sierra Nevada, California, *in* Ernst, W.G., ed., Rubey Volume on the Geotectonic Development of California: Englewood Cliffs, New Jersey, Prentice-Hall, p. 132–181.
Saleeby, J.B., and Sharp, W.D., 1980, Chronology of the structural and petrologic development of the southwest Sierra Nevada foothills, California: Geological Society of America Bulletin, v. 91, Part II, p. 1416–1535, https://doi.org/10.1130/GSAB-P2-91-1416.
Saleeby, J.B., Ducea, M.N., Busby, C., Nadin, E., and Whetmore, P.H., 2008, Chronology of pluton emplacement and regional deformation in the southern Sierra Nevada batholith, California, *in* Wright, J.E., and Shervais, J.W., eds., Ophiolites, Arcs, and Batholiths: Geological Society of America Special Paper 438, p. 397–427, https://doi.org/10.1130/2008.2438(14).
Saltus, R.W., and Jachens, R.C., 1995, Gravity and basin-depth maps of the Basin and Range Province, western United States: U.S. Geological Survey Geophysical Investigations Map GP-1012, 1:2,500,000 scale.
Saltus, R.W., and Thompson, G.A., 1995, Why is it downhill from Tonopah to Las Vegas?: A case for a mantle plume support of the high northern Basin and Range: Tectonics, v. 14, no. 6, p. 1235–1244, https://doi.org/10.1029/95TC02288.
Schellart, W.P., Stegman, D.R., Farrington, R.J., Freeman, J., and Moresi, L., 2010, Cenozoic tectonics of western North America controlled by evolving width of Farallon slab: Science, v. 329, no. 5989, p. 316–319, https://doi.org/10.1126/science.1190366.
Schmandt, B., and Humphreys, E.D., 2011, Seismically imaged relict slab from the 55 Ma Siletzia accretion to the northwest United States: Geology, v. 39, no. 2, p. 175–178, https://doi.org/10.1130/G31558.1.
Schweickert, R.A., 1981, Tectonic evolution of the Sierra Nevada range, in Ernst, W.G., ed., Geotectonic Development of California: Rubey Volume I: Englewood Cliffs, New Jersey, Prentice-Hall, p. 87–131.
Sharp, W., 1988, Pre-Cretaceous crustal evolution of the Sierra Nevada region, California, *in* Ernst, W.G., ed., Geotectonic Development of California: Rubey Volume I: Englewood Cliffs, New Jersey, Prentice-Hall, p. 824–864.
Shaver, S.A., and McWilliams, M., 1987, Cenozoic extension and tilting recorded in Upper Cretaceous and Tertiary rocks at the Hall molybdenum deposit, northern San Antonio Mountains, Nevada: Geological Society of America Bulletin, v. 99, no. 3, p. 341–353, https://doi.org/10.1130/0016–7606(1987)99<341:CEATRI>2.0.CO;2.
Small, E.E., and Anderson, R.S., 1995, Geomorphically driven late Cenozoic rock uplift in the Sierra Nevada, California: Science, v. 270, no. 5234, p. 277–281, https://doi.org/10.1126/science.270.5234.277.
Sonder, L.J., and Jones, C.H., 1999, Western United States extension: How the west was widened: Annual Review of Earth and Planetary Sciences, v. 27, p. 417–462, https://doi.org/10.1146/annurev.earth.27.1.417.
Sousa, F.J., 2019, Eocene Origin of Owens Valley, California: Geosciences, v. 9, no. 5, p. 194–207, https://doi.org/10.3390/geosciences9050194.
Stern, T.W., Bateman, P.C., Morgan, B.A., Newell, M.F., and Peck, D.L., 1981, Isotopic U-Pb ages of zircon from the granitoids of the central Sierra Nevada: U.S. Geological Survey Professional Paper 1185, 17 p., https://doi.org/10.3133/pp1185.
Stock, G.M., Anderson, R.S., and Finkel, R.C., 2004, Pace of landscape evolution in the Sierra Nevada, California, revealed by cosmogenic dating of cave sediments: Geology, v. 32, no. 3, p. 193–196, https://doi.org/10.1130/G20197.1.
Stockli, D.F., 1999, Regional timing and spatial distribution of Miocene extension in the northern Basin and Range Province [Ph.D. thesis]: Stanford, California, Stanford University, 239 p.
Stockli, D.F., Farley, K.A., and Dumitru, T.A., 2000, Calibration of the apatite (U-Th)/He thermochronometer on an exhumed fault block, White Mountains, California: Geology, v. 28, no. 11, p. 983–986, https://doi.org/10.1130/0091-7613(2000)28<983:COTAHT>2.0.CO;2.
Stockli, D.F., Linn, J.K., Walker, J.D., and Dumitru, T.A., 2001, Miocene unroofing of the Canyon Range during extension along the Sevier Desert Detachment, west-central Utah: Tectonics, v. 20, p. 289–307, https://doi.org/10.1029/2000TC001237.
Stockli, D.F., Surpless, B.E., Dumitru, T.A., and Farley, K.A., 2002, Thermochronological constraints on the timing and magnitude of Miocene and Pliocene extension in the central Wassuk Range, western Nevada: Tectonics, v. 21, p. 10–19, https://doi.org/10.1029/2001TC001295.

Stockli, D.F., Dumitru, T.A., McWilliams, M.O., and Farley, K.A., 2003, Cenozoic tectonic evolution of the White Mountains, California and Nevada: Geological Society of America Bulletin, v. 115, no. 7, p. 788–816, https://doi.org/10.1130/0016-7606(2003)115<0788:CTEOTW>2.0.CO;2.

Stone, P., Dunne, G.C., Moore, J.G., and Smith, G.I., 2000, Geologic map of the Lone Pine 15′ quadrangle, Inyo County, California: U.S. Geological Survey I-2617, scale 1:62,500, https://doi.org/10.3133/i2617.

Surpless, B., Stockli, D.F., Dumitru, T.A., and Miller, E.L., 2002, Two-phase westward encroachment of Basin and Range extension into the northern Sierra Nevada: Tectonics, v. 21, p. 1002–1014, https://doi.org/10.1029/2000TC001257.

Tincher, C.R., and Stockli, D.F., 2009, Cenozoic volcanism and tectonics in the Queen Valley area, Esmeralda County, western Nevada, *in* Oldow, J.S., and Cashman, P.H., eds., Late Cenozoic Structure and Evolution of the Great Basin–Sierra Nevada Transition: Geological Society of America Special Paper 447, https://doi.org/10.1130/2009.2447(13).

Thompson, G.A., and Parsons, T., 2009, Can footwall unloading explain late Cenozoic uplift of the Sierra Nevada crest?: International Geology Review, v. 51, no. 9–11, p. 986–993, https://doi.org/10.1080/00206810903059156.

Unruh, J.R., 1991, The uplift of the Sierra Nevada and implications for late Cenozoic epeirogeny in the western Cordillera: Geological Society of America Bulletin, v. 103, no. 11, p. 1395–1404, https://doi.org/10.1130/0016-7606(1991)103<1395:TUOTSN>2.3.CO;2.

Unruh, J.R., Humphrey, J., and Barron, A., 2003, Transtensional model for the Sierra Nevada Frontal fault system, eastern California: Geology, v. 31, no. 4, p. 327–330, https://doi.org/10.1130/0091-7613(2003)031<0327:TMFTSN>2.0.CO;2.

Vening Meinesz, F., 1950, Les grabens africains, resultat de compression ou de tension dans la croûte terrestre?: Institut Royal Colonial Belge: Bulletin des Seances, v. 21, p. 539–552.

Wakabayashi, J., 2013, Paleochannels, stream incision, erosion, topographic evolution, and alternative explanations of paleoaltimetry, Sierra Nevada, California: Geosphere, v. 9, no. 2, p. 191–215, https://doi.org/10.1130/GES00814.1.

Wakabayashi, J., and Sawyer, T.L., 2001, Stream incision, tectonics, uplift and evolution of topography of the Sierra Nevada, California: The Journal of Geology, v. 109, no. 5, p. 539–562, https://doi.org/10.1086/321962.

Walker, J.D., Tandis, S.B., Didericksen, B.D., Stockli, D.F., and Andrew, J.E., 2014, Middle Miocene to recent exhumation of the Slate Range, eastern California, and implications for the timing of extension and the transition to transtension: Geosphere, v. 10, no. 2, no. 9, p. 276–291, https://doi.org/10.1130/GES00947.1.

Wells, R.E., and McCaffrey, R., 2013, Steady rotation of the Cascade arc: Geology, v. 41, no. 9, p. 1027–1030, https://doi.org/10.1130/G34514.1.

Wernicke, B., and Axen, G.J., 1988, On the role of isostasy in the evolution of normal fault systems: Geology, v. 16, no. 9, p. 848–851, https://doi.org/10.1130/0091-7613(1988)016<0848:OTROII>2.3.CO;2.

Wernicke, B., and Snow, J.K., 1998, Cenozoic tectonism in the central Basin and Range; motion of the Sierran-Great Valley Block: International Geology Review, v. 40, p. 403–410, https://doi.org/10.1080/00206819809465217.

Wernicke, B.P., Clayton, R., Ducea, M., Jones, C.H., Park, S., Ruppert, S., Saleeby, J., Snow, J.K., Squires, L., Fliedner, M., Jiracek, G., Keller, R., Klemperer, S., Luetgert, J., Malin, P., Miller, K., Mooney, W., Oliver, H., and Phinney, R., 1996, Origin of high mountains in the continents: The southern Sierra Nevada: Science, v. 271, no. 5246, p. 190–193, https://doi.org/10.1126/science.271.5246.190.

Wolf, R.A., Farley, K.A., and Silver, L.T., 1996, Helium diffusion and low temperature thermochronometry of apatite: Geochimica et Cosmochimica Acta, v. 60, p. 4231–4240, https://doi.org/10.1016/S0016-7037(96)00192-5.

Wolf, R.A., Farley, K.A., and Kass, D.M., 1998, Modeling of the temperature sensitivity of the apatite (U-Th)/He thermochronometer: Chemical Geology, v. 148, no. 1–2, p. 105–114, https://doi.org/10.1016/S0009-2541(98)00024-2.

Wolfe, J.A., Schorn, H.E., Forest, C.E., and Molnar, P., 1997, Paleobotanical evidence for high altitudes in Nevada during the Miocene: Science, v. 276, p. 1672–1675, https://doi.org/10.1126/science.276.5319.1672.

Wright, L., 1976, Late Cenozoic fault patterns and stress fields in the Great Basin and westward displacement of the Sierra Nevada block: Geology, v. 4, no. 8, p. 489–494, https://doi.org/10.1130/0091-7613(1976)4<489:LCFPAS>2.0.CO;2.

Yeend, W.R., 1974, Gold-bearing gravels of the ancestral Yuba River, Sierra Nevada, California: U.S. Geological Survey Professional Paper 772, 44 p., https://doi.org/10.3133/pp772.

Zandt, G., and Humphreys, E., 2008, Tordoidal mantle flow through the western U.S. slab window: Geology, v. 36, no. 4, p. 295–298, https://doi.org/10.1130/G24611A.1.

Zandt, G., Gilbert, H., Owens, T.J., Ducea, M., Saleeby, J., and Jones, C.H., 2004, Active foundering of a continental arc root beneath the southern Sierra Nevada in California: Nature, v. 431, p. 41–46, https://doi.org/10.1038/nature02847.